

Ca²⁺-Dependent Gating Mechanisms for *dSlo*, a Large-Conductance Ca²⁺-Activated K⁺ (BK) Channel

Brenda L. Moss,* Shai D. Silberberg,# Crina M. Nimigean,* and Karl L. Magleby*

*Department of Physiology and Biophysics, University of Miami School of Medicine, Miami, Florida 33101-6430 USA; and #Department of Life Sciences and the Zlotowski Center for Neuroscience, Ben Gurion University of the Negev, Beer-Sheva 84105, Israel

ABSTRACT The Ca²⁺-dependent gating mechanism of cloned BK channels from *Drosophila* (*dSlo*) was studied. Both a natural variant (A1/C2/E1/G3/I0) and a mutant (S942A) were expressed in *Xenopus* oocytes, and single-channel currents were recorded from excised patches of membrane. Stability plots were used to define stable segments of data. Unlike native BK channels from rat skeletal muscle in which increasing internal Ca²⁺ concentration (Ca_i²⁺) in the range of 5 to 30 μM increases mean open time, increasing Ca_i²⁺ in this range for *dSlo* had little effect on mean open time. However, further increases in Ca_i²⁺ to 300 or 3000 μM then typically increased *dSlo* mean open time. Kinetic schemes for the observed Ca²⁺-dependent gating kinetics of *dSlo* were evaluated by fitting two-dimensional dwell-time distributions using maximum likelihood techniques and by comparing observed dependency plots with those predicted by the models. Previously described kinetic schemes that largely account for the Ca²⁺-dependent kinetics of native BK channels from rat skeletal muscle did not adequately describe the Ca²⁺ dependence of *dSlo*. An expanded version of these schemes which, in addition to the Ca²⁺-activation steps, permitted a Ca²⁺-facilitated transition from each open state to a closed state, could approximate the Ca²⁺-dependent kinetics of *dSlo*, suggesting that Ca²⁺ may exert dual effects on gating.

INTRODUCTION

Large-conductance Ca²⁺-activated potassium channels (BK or maxi-K⁺ channels) are activated by both intracellular Ca²⁺ and membrane depolarization. Consequently, BK channels provide a direct link between Ca²⁺-dependent cellular processes and membrane potential (reviewed by McManus, 1991; Latorre, 1994). BK channels have been observed in a wide variety of cell types where they play crucial roles in many different physiological processes including neurotransmitter release (Robitaille et al., 1993), secretion (Petersen and Maruyama, 1984), smooth muscle contraction (Nelson et al., 1995), and the electrical tuning of cochlear hair cells (Hudspeth and Lewis, 1988; Wu et al., 1995).

Considerable progress has been made toward understanding the Ca²⁺-dependent gating mechanism of BK channels due to their unusually large conductance (150–350 pS in symmetrical 150 mM KCl), which allows single-channel currents to be recorded with high time resolution. For example, the minimal model of McManus and Magleby (1991) and an expanded version of this model with additional brief closed states (Rothberg and Magleby, 1998) can account for the major features of the Ca²⁺-dependent single-channel kinetics of native BK channels in rat skeletal muscle from low to moderate levels of Ca_i²⁺. Wu et al. (1995) were able to account for the activity of native BK

channels in turtle cochlear hair cells by expanding the minimal model of McManus and Magleby (1991) with two additional closed states (denoted as Ca²⁺-blocked states) beyond the open states.

The recent cloning of the BK channel pore-forming α subunit, first from *Drosophila* (*dSlo*) (Atkinson et al., 1991; Adelman et al., 1992), and later from other species, has allowed investigators to study BK channels of known primary structure (DiChiara and Reinhart, 1995; McManus et al., 1995; Silberberg et al., 1996; Cox et al., 1997; Schreiber and Salkoff, 1997; Stefani et al., 1997). However, compared to native BK channels, much less is known about the detailed single-channel kinetics of cloned BK channels.

The purpose of the present study was to characterize the Ca²⁺-dependent single-channel kinetics of *dSlo* and to work toward developing a kinetic scheme that could account for the observed effects of Ca_i²⁺. We found that, unlike native BK channels in rat skeletal muscle where increases in Ca_i²⁺ lead to progressive increases in mean open time, increases to intermediate Ca_i²⁺ (30 μM) for *dSlo* had little effect on mean open time. Further increases to higher Ca_i²⁺ (300 or 3000 μM) for *dSlo* then typically increased mean open time. Kinetic schemes for the observed single-channel gating were evaluated by fitting two-dimensional (2-D) dwell-time distributions using maximum likelihood techniques. Results indicate that the models, which largely account for the Ca²⁺-dependent kinetics of native BK channels from rat skeletal muscle, do not adequately describe the Ca²⁺-dependent single-channel kinetics of *dSlo*. However, an extension of the models of McManus and Magleby (1991) and Wu et al. (1995), which permits a Ca²⁺-facilitated transition from each open state to a brief closed state, can approximate the Ca²⁺-dependent kinetics of *dSlo*. A preliminary report of some of these findings has appeared (Moss et al., 1998).

Received for publication 10 November 1998 and in final form 3 March 1999.

Address reprint requests to Dr. Karl L. Magleby, Department of Physiology and Biophysics, University of Miami School of Medicine, P.O. Box 016430, Miami, FL 33101-6430. Tel.: 305-243-6236; Fax: 305-243-6898; E-mail: kmagleby@miami.edu.

© 1999 by the Biophysical Society

0006-3495/99/06/3099/19 \$2.00

MATERIALS AND METHODS

Expression of *dSlo* channels in *Xenopus* oocytes

Xenopus laevis oocytes were enzymatically separated using collagenase as previously described (Dahl, 1992). Earlier work had suggested that *dSlo* channels expressed in *Xenopus* oocytes may be modulated by an endogenous cyclic AMP-dependent protein kinase (PKA)-like protein, which remains functionally associated with the channels in excised patches (Esguerra et al., 1994; see Bowlby and Levitan, 1996). Therefore, oocytes were microinjected with either cRNA transcribed in vitro from cDNA encoding variant A1/C2/E1/G3/I0 of *dSlo* (wild-type channel) (Adelman et al., 1992) or with cRNA in which a putative PKA phosphorylation site was eliminated by replacing serine at position 942 with alanine (S942A channel), as described previously (Esguerra et al., 1994). Single-channel currents from expressed BK channels were recorded in excised patches of membrane 2–4 days after microinjecting 2–10 ng of cRNA.

Single-channel recording

Currents were recorded from *dSlo* channels using the inside-out configuration of the patch-clamp technique (Hamill et al., 1981) as described previously (Silberberg et al., 1996). Unless otherwise indicated, experiments were performed on patches containing a single S942A channel, determined by extended recordings at levels of Ca_i^{2+} that would be expected to readily activate BK channels. *Xenopus* oocytes can express very low levels of endogenous BK channels (Krause et al., 1996). However, the single-channel currents in the present study are unlikely to have arisen from endogenous BK channels since these channels are apparently activated at lower Ca_i^{2+} than was observed for the *dSlo* channels studied here. Also, single *dSlo* channels (variant A1/C2/E1/G3/I0) are characterized by a very distinctive gating pattern in which channel openings are interrupted by numerous brief closings, or “flickers,” in contrast to the much lower frequency of flickers in the records of Krause et al. (1996).

For the experiments on *dSlo*, the pipette (extracellular) solution contained (in mM): potassium gluconate, 154; KCl, 6; $CaCl_2$, 1; $MgCl_2$, 1; TES buffer (*N*-tris (hydroxymethyl)methyl-2-aminoethane sulfonic acid), 5. The microchamber (intracellular) solution contained (in mM): potassium gluconate, 150; KCl, 10; TES buffer, 5; and sufficient $CaCl_2$ to achieve the desired levels of free calcium. Solutions were adjusted to pH 7.0. The method used to estimate the buffering capacity of gluconate for Ca^{2+} is detailed in Silberberg et al. (1996). The data presented from native BK channels in rat skeletal muscle were from previous experiments carried out in symmetrical 144–150 mM KCl with 5 mM TES pH buffer, and using various methods to set Ca_i^{2+} (details in McManus and Magleby, 1991; Rothberg and Magleby, 1998).

The membrane potential of the excised patches was held at +30 mV (intracellular side positive). Current records were effectively low-pass filtered at 6.5–9 kHz (–3 dB) as indicated in the figure legends. Experiments were performed at room temperature (21–23°C).

Sampling and measuring interval durations

Single-channel current records were sampled at 100–200 kHz, durations of open and closed intervals were measured with half-amplitude threshold analysis, and stability plots were constructed as described in detail previously for *dSlo* (Silberberg et al., 1996) and native BK channels (McManus and Magleby, 1988, 1991).

Two of the four experiments examining the effect of high Ca_i^{2+} on mean open time (and no other kinetic parameters) were performed on patches containing two *dSlo* channels. Mean open time was determined from the upper level with two channels open by multiplying the measured open duration for this level by two, as either channel could close. This result was in agreement with the estimates of mean open time obtained directly from the lower level.

Log-binning and plotting one-dimensional (1-D) dwell-time distributions

The methods used to log bin the intervals into 1-D dwell-time distributions, fit the distributions with sums of exponentials using maximum likelihood fitting techniques (intervals less than two dead times were excluded from the fitting), determine the number of significant exponential components with the likelihood ratio test, and generate simulated current records with filtering and noise have been described previously (Blatz and Magleby, 1986; McManus and Magleby, 1988, 1991; Colquhoun and Sigworth, 1995). Dwell-time distributions are plotted with the Sigworth and Sine (1987) transformation, as the square root of the number of intervals per bin, without correcting for the logarithmic increase in bin width with time.

Log-binning and plotting 2-D dwell-time distributions

The theory of 2-D dwell-time distributions can be found in Fredkin et al. (1985), Keller et al. (1990), and Rothberg et al. (1997). Two-dimensional dwell-time distributions were generated as detailed in Rothberg and Magleby (1998), and plotted by extending the Sigworth and Sine (1987) transformation to 2-D dwell-time distributions. Briefly, every open interval and its following (adjacent) closed interval were binned as well as every closed interval and its following (adjacent) open interval, with the logs of the open and closed interval durations of each pair locating the bin on the *y* and *x* axes, respectively. The 2-D surface plots were generated with the program Surfer (Golden Software, Golden, CO).

Dependency plots

Dependency plots were constructed from the 2-D dwell-time distributions as described in Magleby and Song (1992). The dependency for each bin of open-closed interval pairs with mean durations t_o and t_c is:

$$\text{Dependency}(t_o, t_c) = \frac{N_{\text{obs}}(t_o, t_c) - N_{\text{ind}}(t_o, t_c)}{N_{\text{ind}}(t_o, t_c)} \quad (1)$$

where $N_{\text{obs}}(t_o, t_c)$ is the observed number of interval pairs in bin (t_o, t_c) , and $N_{\text{ind}}(t_o, t_c)$ is the calculated number of interval pairs in bin (t_o, t_c) if adjacent open and closed intervals pair independently (at random). The expected number of interval pairs in bin (t_o, t_c) for independent pairing is:

$$N_{\text{ind}}(t_o, t_c) = P(t_o) \times P(t_c) \quad (2)$$

where $P(t_o)$ is the probability of an open interval falling in the row of bins with a mean open duration of t_o , and $P(t_c)$ is the probability of a closed interval falling in the column of bins with a mean closed duration of t_c . $P(t_o)$ is given by the number of open intervals in row t_o divided by the total number of open intervals, and $P(t_c)$ is given by the number of closed intervals in column t_c divided by the total number of closed intervals. To facilitate comparison between experimental and predicted dependency plots, data simulated from the models contained the same number of intervals as in the corresponding experimental data.

Estimating the most likely rate constants for kinetic schemes

The most likely rate constants for the examined kinetic schemes were determined from fitting 2-D frequency histograms (dwell-time distributions) obtained at either a single Ca_i^{2+} or simultaneously fitting distributions obtained at three or four different Ca_i^{2+} . Fitting was done using an iterative maximum likelihood fitting procedure similar to the one detailed in McManus and Magleby (1991), except that 2-D dwell-time distributions replaced the 1-D dwell-time distributions, and the correction method of Crouzy and Sigworth (1990) for missed events due to filtering replaced our previous correction method. Additional details of the fitting including the

methods used to correct for missed events are given in Rothberg and Magleby (1998).

Evaluating and ranking the kinetic schemes

Normalized likelihood ratios (NLR) were used to compare the ability of any given kinetic scheme to describe the experimental 2-D dwell-time distributions to the description given by the theoretical best fit (McManus and Magleby, 1991; Rothberg and Magleby, 1998). Normalization accounts for the differences in numbers of interval pairs among experiments, so that comparisons can be made among channels. The normalized likelihood ratio per 1000 interval pairs, NLR_{1000} , is defined as:

$$NLR_{1000} = \exp((\ln S - \ln T)(1000/N)) \quad (3)$$

where $\ln S$ is the natural logarithm of the maximum likelihood estimate for the observed 2-D dwell-time distributions given the kinetic scheme, $\ln T$ is the natural logarithm of the maximum-likelihood estimate for the theoretical best description of the observed distributions with sums of 2-D exponential components, and N is the total number of fitted interval pairs in the observed dwell-time distributions. The theoretical best description of the dwell-time distributions was estimated by fitting the 2-D dwell-time distributions with sums of 2-D exponential components with all free parameters, except for the volume of one component, since the volumes of the components must sum to 1.0. The number of components was increased until there was no longer a significant increase in likelihood. The maximum likelihood for this fit would then approximate that of the theoretical best description for a discrete-state Markov model that generates the same number of exponential components fit to the same data (Rothberg et al., 1997).

Although the NLR_{1000} gives a measure of how well different kinetic schemes describe the data, it cannot be used directly for ranking schemes since no penalty is applied for the number of free parameters. To overcome this difficulty, the Schwarz criterion was used to apply penalties and rank models (detailed in McManus and Magleby, 1991). The Schwarz criterion (SC) is given by

$$SC = -L + (0.5 F)(\ln N) \quad (4)$$

where L is the natural logarithm of the maximum likelihood estimate, F is the number of free parameters, and N is the number of intervals. The scheme with the smallest SC is ranked first.

RESULTS

Currents recorded from single *dSlo* channels

Currents recorded from a single *dSlo* channel in an excised patch of membrane from a *Xenopus* oocyte are shown in Fig. 1, *A* and *D* on slow and fast time bases, respectively. Openings (upward current steps) separated by very brief closed intervals are grouped into bursts separated by longer closed intervals. Occasional isolated openings of brief duration also occur. Such complex activity is consistent with entry into multiple open and closed states during gating, as described previously for native BK channels from skeletal muscle (reviewed by McManus, 1991; Latorre, 1994). The objective of this study is to work toward developing a kinetic gating mechanism that can account for this single-channel activity of *dSlo*.

Stability plots can be used to define stable segments of data from *dSlo* channels

The open probability (P_O) of cloned *dSlo* channels expressed in *Xenopus* oocytes is often less stable than that of

native BK channels in cultured rat skeletal muscle (Silberberg et al., 1996; Bowlby and Levitan, 1996). Therefore, precautions were taken to obtain stable data for analysis. Only channels in which P_O appeared relatively stable for at least 10 min were selected for initial analysis. Each channel was then analyzed with stability plots (Blatz and Magleby, 1986) to examine the stability of the kinetic properties as well as to identify moding and subconductance levels (McManus and Magleby, 1988).

The process used to select stable data for analysis from one *dSlo* channel is shown in Fig. 1. Fig. 1 *A* presents consecutive single-channel current traces for 10 continuous minutes of recording. Fig. 1 *B* shows stability plots of the open (*top*) and closed (*bottom*) intervals from the record in Fig. 1 *A*. Each line segment plots the average duration of 150 consecutive open or closed intervals. For 90% of the intervals (~40,000 of the 44,500 total open and closed intervals), both the mean open time and mean closed time remained relatively constant, suggesting stable channel kinetics. This predominant type of activity will be referred to as normal mode activity. The remaining 10% of the intervals was associated with three distinct kinetic modes other than normal. The modes labeled 1 and 2 in Fig. 1 *B* were characterized by abrupt decreases in both mean open time and mean closed time. The mode labeled 3 was characterized by a decrease in mean closed time with no corresponding change in mean open time. The variation in P_O due to moding is apparent in Fig. 1 *C*.

Inspection of the current record corresponding to mode 1 revealed that the channel generated a burst of very brief open and closed intervals (Fig. 1 *D*, *1*) similar to the buzz mode described for native BK channels in cultured rat skeletal muscle (McManus and Magleby, 1988). During mode 2, the channel opened to a subconductance level of ~40% of the normal open level (Fig. 1 *D*, *2*). Mode 3 was associated with a decreased duration of the shut intervals (not shown).

Intervals occurring during sojourns to modes other than normal were excluded from the analysis, and the resulting stability plots for the remaining open and closed intervals are shown in Fig. 1 *E*. These data represent activity in the normal mode. The moving means fluctuate about the overall means of 2.5 ms for the open intervals and 29.6 ms for the closed intervals (*dashed lines*). A fluctuation of the mean responses about the overall means during normal activity is expected due to stochastic variation in the open and closed interval durations (Blatz and Magleby, 1986). The fluctuations of the closed intervals about the mean during normal activity are greater than those of the open intervals because the range of durations of closed intervals averaged for each segment was greater. Fig. 1 *F* presents the corresponding stability plot of P_O during normal activity. The stability plots in Fig. 1, *E* and *F* are consistent with relatively stable kinetics during normal mode activity, as there is no indication of long-term drift in the running means.

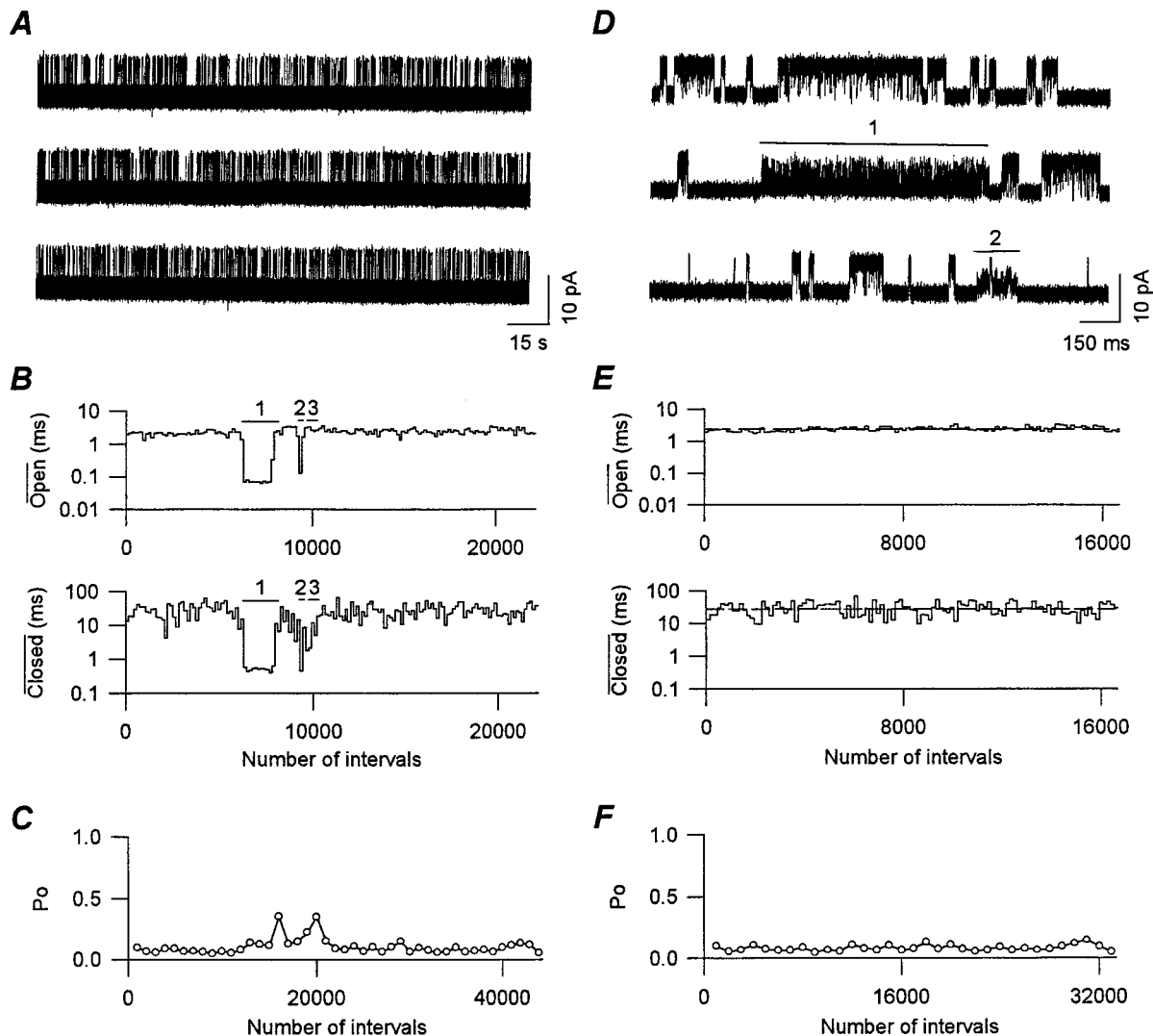


FIGURE 1 Defining segments of data with stable kinetic properties from a single *dSlo* channel. (A) Consecutive single-channel current traces for 10 continuous minutes of recording from a *dSlo* channel in an excised patch of membrane. Upward (outward) currents indicate channel opening. (B) Stability plots of the 44,500 detected open (top) and closed (bottom) intervals from the current record shown in A. Each line segment represents the average duration of 150 consecutive open or closed intervals. Bars labeled 1, 2, and 3 indicate transitions to modes. (C) Plot of P_o as a function of interval number for the current record in A. Each point represents the average of 1000 consecutive open and closed intervals. (D) Excerpts of current records from A presented on an expanded time scale showing a buzz-like mode (1) and openings to a subconductance level (2). The numbers over modes 1 and 2 correspond to the labeling in B. (E) Stability plots for the current record in A after transitions to subconductance levels and modes other than normal were excluded. This exclusion removed $\sim 10\%$ of the detected intervals in this experiment. Mean interval durations over the entire data set are shown by the dashed lines. (F) Plot of P_o versus interval number for the data in E. Effective low-pass filtering of 7 kHz; $11 \mu\text{M Ca}_i^{2+}$. Data for this figure and the rest of the paper were obtained at a membrane potential of $+30 \text{ mV}$. Channel H23.

Recordings were obtained from a total of 53 excised patches (39 S942A and 14 wild-type), each containing a single *dSlo* channel. Thirty-nine of these channels were rejected because the stable number of intervals was insufficient for analysis or because of large fluctuations in P_o over time, suggestive of wanderlust kinetics (Silberberg et al., 1996; Bowlby and Levitan, 1996). The results presented in this paper were obtained from the remaining 14 *dSlo* channels (12 S942A and 2 wild-type). Although most of the channels studied were S942A, there was no obvious indication that wild-type channels were less stable than the mutant (Silberberg et al., 1996) or had different kinetics.

The data were initially analyzed as described above to obtain stable segments of data during normal activity. Data from individual channels were analyzed separately, because *dSlo* channels encoded by the same cDNA may display variable calcium sensitivity (Silberberg et al., 1996).

Increasing Ca_i^{2+} from 5 to 30 μM has little effect on mean open time

Fig. 2, A and C presents currents recorded through a single *dSlo* channel at two different Ca_i^{2+} . Increasing Ca_i^{2+} from

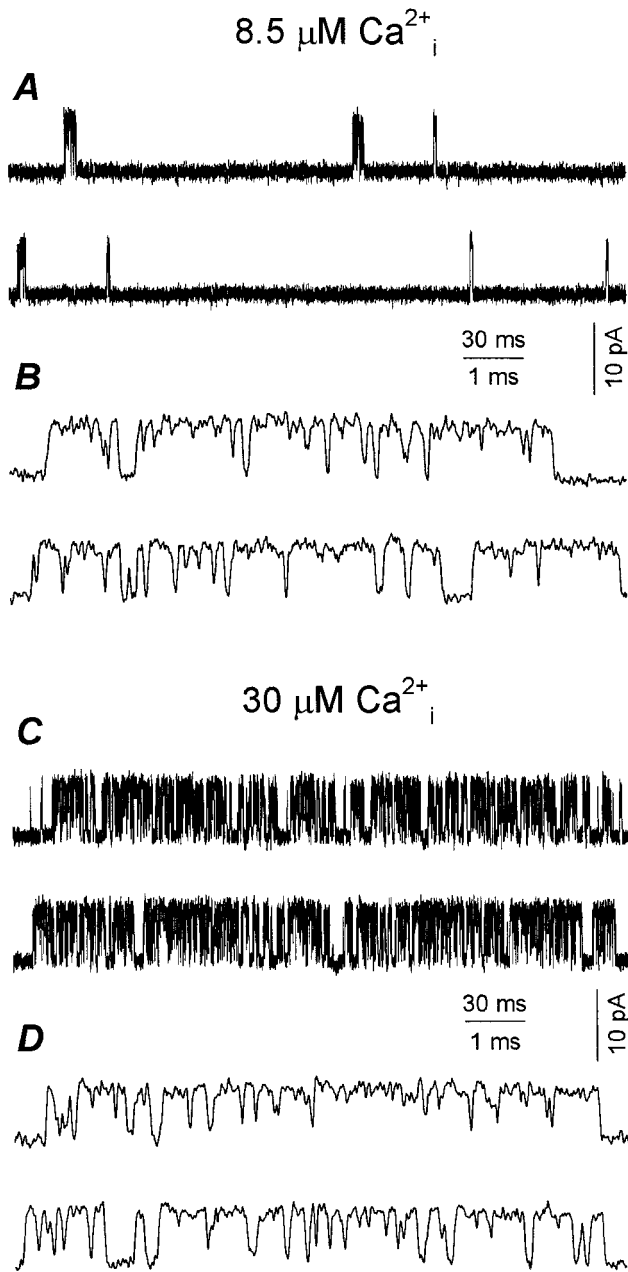


FIGURE 2 Increasing Ca_i^{2+} from 8.5 to 30 μM markedly decreases the closed interval durations while having little effect on the open interval durations. Currents recorded from a single *dSlo* channel at the indicated Ca_i^{2+} . Data are presented on a slow time base in (A) and (C) and on a faster time base in (B) and (D). Effective low-pass filtering of 9 kHz. Channel H06.

8.5 μM to 30 μM increased P_O (from 0.10 to 0.69), as would be expected for a BK channel. This increase in P_O was associated with a marked decrease in the durations of closed intervals separating bursts of openings, consistent with results described previously for both native and cloned BK channels (McManus and Magleby, 1991; Adelman et al., 1992; DiChiara and Reinhart, 1995).

Fig. 2, B and D presents currents recorded from the same *dSlo* channel, but on a faster time base so that open intervals

within bursts of openings can be resolved. Surprisingly, the open interval durations appeared little changed when Ca_i^{2+} was increased to 30 μM . This apparent insensitivity of *dSlo* open interval duration to increasing Ca_i^{2+} contrasts to the observed increase in open interval duration with increasing Ca_i^{2+} reported for native rat skeletal muscle BK channels (McManus and Magleby, 1991).

To further examine the apparent insensitivity of open interval duration to increasing Ca_i^{2+} , mean open interval durations were measured and plotted against Ca_i^{2+} for five *dSlo* channels. As shown in Fig. 3 A, mean open time remained relatively constant (with a suggestion of a slight decrease) over the examined range of Ca_i^{2+} (5–30 μM).

For comparison, Fig. 3 C plots mean open time versus Ca_i^{2+} for eight BK channels from previous experiments on cultured rat skeletal muscle. In contrast to the apparent insensitivity of *dSlo* channel mean open time to increasing Ca_i^{2+} , the mean open time of all eight native BK channels increased dramatically (~2–3-fold) over a similar range of Ca_i^{2+} . The difference in response was not due to differences in filtering, as three of the eight channels in Fig. 3 C had levels of filtering similar to those used in Fig. 3 A, and the relatively flat response in Fig. 3 A was still observed when the level of filtering was increased to be similar to that of the more heavily filtered channels in Fig. 3 C (not shown).

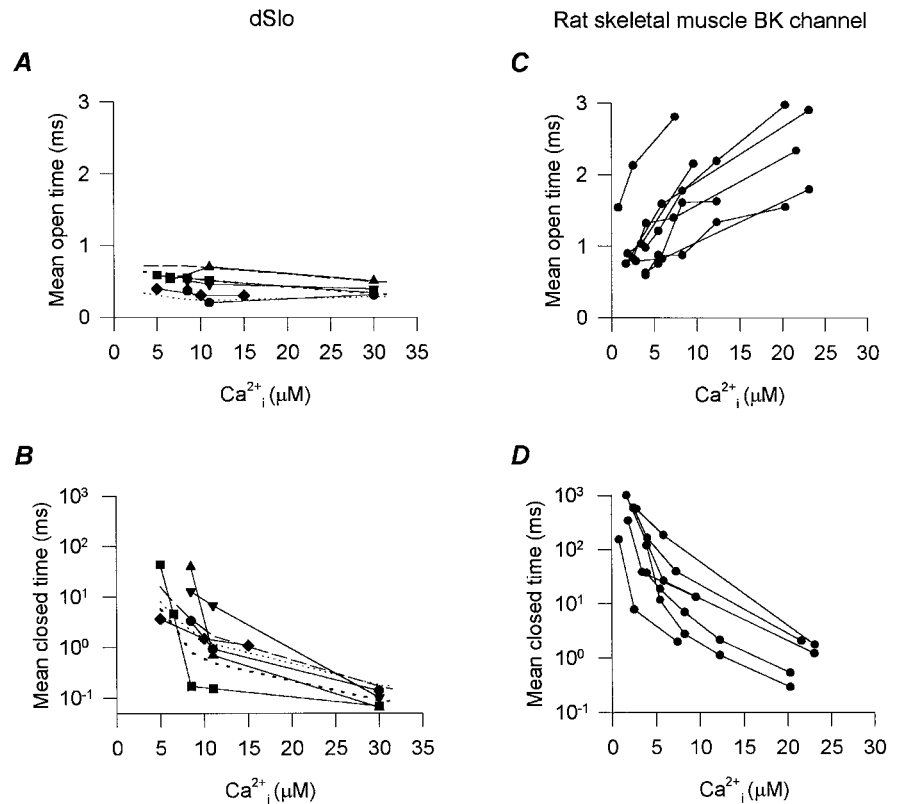
The major anion in the solutions for the experiments on *dSlo* was gluconate⁻ to eliminate currents through Ca²⁺-activated Cl⁻ channels present in oocytes. This differs from Cl⁻ used as the major anion for the previous experiments on native rat skeletal muscle BK channels. However, the difference in response is unlikely to be due to the difference in anion, as BK channels cloned from mouse (*mSlo*) and expressed in oocytes using gluconate⁻ as the major anion show an increase in mean open time with increasing Ca_i^{2+} , similar to that observed for native skeletal muscle BK channels (B. L. Moss, unpublished observations, three of three examined *mSlo* channels). Thus, the gating of *dSlo* differs from that of both *mSlo* and BK channels in rat skeletal muscle.

In contrast to the differential effects of increasing Ca_i^{2+} on the mean open time of *dSlo* and native skeletal muscle BK channels, increasing Ca_i^{2+} consistently decreased mean closed time for both types of BK channels, as shown in Fig. 3, B and D.

Effect of Ca_i^{2+} on the 1-D dwell-time distributions

Fig. 4 presents 1-D dwell-time distributions of open and closed interval durations obtained from a single *dSlo* channel at two different Ca_i^{2+} . Increasing Ca_i^{2+} from 8.5 to 30 μM had little effect on the open intervals and shifted the closed intervals from longer to briefer durations. The lines plot the maximum likelihood fits with sums of exponentials. Each of the open distributions was well-described by the sum of three significant exponential components and the closed distributions were described by the sums of six (8.5

FIGURE 3 Increasing Ca_i^{2+} has little effect on the mean open times of *dSlo*, increases the mean open time of native BK channels from rat skeletal muscle, and decreases the mean closed times of both channels. Mean open and mean closed time plotted against Ca_i^{2+} for five *dSlo* channels (A and B) and eight native BK channels from cultured rat skeletal muscle (C and D). Four of the *dSlo* channels were S942A and one was wild-type (channel H01, \blacklozenge). Effective low-pass filtering of 9 kHz for the *dSlo* channels and 6–10 kHz for the skeletal muscle BK channels. P_O ranged from 0.013 to 0.89 for *dSlo* and from 0.00075 to 0.85 for native BK channels in skeletal muscle. The dashed lines in A and B are the predicted mean open and closed times for Scheme 2. Channel H06, circles and dotted line; channel H08, squares and medium dashes; channel H10, triangles and long dashes.



μM) and five (30 μM) significant exponential components (detailed in figure legend). Similar shifts were observed for each of the other four *dSlo* channels shown in Fig. 3, A and B over the range of examined Ca_i^{2+} .

Minimum number of kinetically distinct states

The number of significant exponential components required to describe the dwell-time distributions of open and closed intervals gives an estimate of the minimum number of kinetic open and closed states (Colquhoun and Hawkes, 1981). Estimates of the number of significant open and closed exponential components for data from 10 *dSlo* channels are presented in Fig. 5. The estimates are plotted against the number of intervals analyzed for each distribution, since the number of significant exponential components can increase with increasing numbers of intervals due to increased resolution to separate exponential components (McManus and Magleby, 1988). The open dwell-time distributions were typically described by the sum of three significant exponential components, and the closed dwell-time distributions were typically described by the sums of five to seven significant exponential components. This suggests that *dSlo* channels typically enter at least three open and five to seven closed kinetic states during normal activity, as do native BK channels in rat skeletal muscle (McManus and Magleby, 1988).

Increasing Ca_i^{2+} to high concentrations (300–3000 μM) can increase mean open time

Increasing Ca_i^{2+} from 5 to 30 μM had little effect on mean open time (Fig. 3 A). To investigate whether open channel block by Ca^{2+} might be masking a Ca^{2+} -induced increase in mean open time, we recorded from *dSlo* channels at low and high Ca_i^{2+} . Fig. 6 presents currents recorded from a single *dSlo* channel in an experiment of this type. Increasing Ca_i^{2+} from 11 to 3000 μM increased mean open time from 2.5 to 8.6 ms. While it is not known how many, if any, of the closings might arise from Ca^{2+} block, if only 10% of the closings in 11 μM Ca_i^{2+} were due to simple Ca^{2+} block, then the 270-fold increase in Ca_i^{2+} should have decreased the mean duration of open intervals ~ 28 -fold. Clearly, no such decrease is observed in Fig. 6. (The filtering was greater for the experiment shown in Fig. 6 than for those shown in Fig. 3 A, and this contributed to the increased mean open time obtained in Fig. 6 at 11 μM Ca_i^{2+} when compared to the mean open times in Fig. 3 A. Increasing the filtering for the data in Fig. 3 A (for three of the examined channels) increased the mean open times into the range of those observed in Fig. 6, while having little effect on the slopes of the relationship between Ca_i^{2+} and mean open time).

In four experiments of the type shown in Fig. 6, increasing Ca_i^{2+} from low levels (≤ 30 μM) to very high levels (300–3000 μM) either had little effect on mean open time (one experiment) or increased mean open time 2–3-fold as

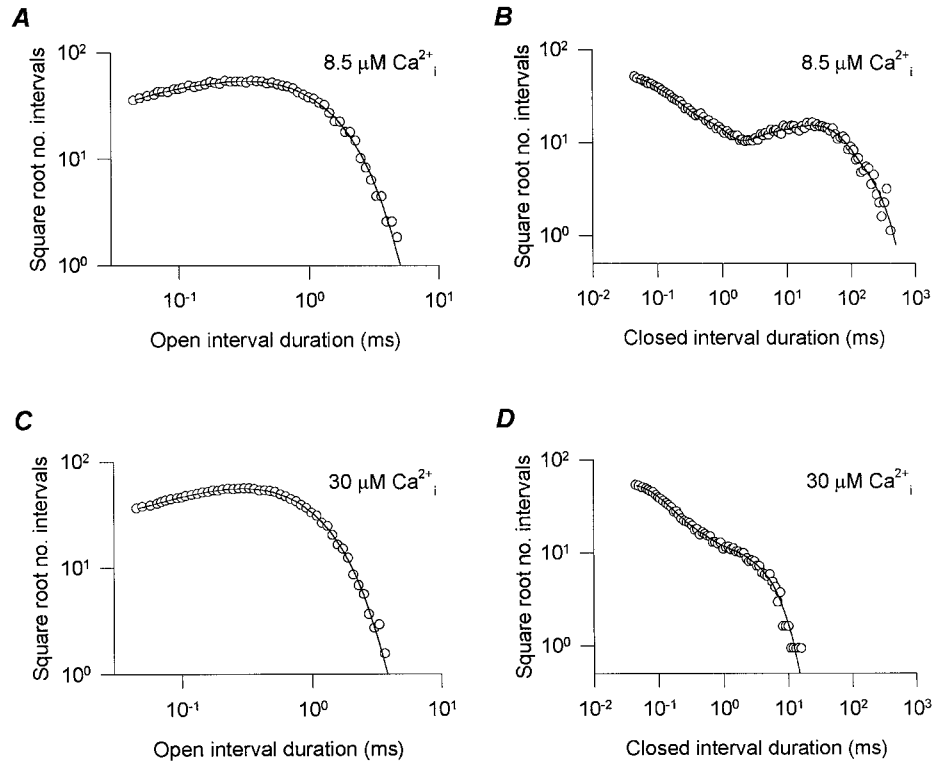


FIGURE 4 Increasing Ca_i²⁺ shifts the 1-D closed dwell-time distribution to shorter durations while having little effect on the open dwell-time distribution. Distributions of open and closed interval durations for data obtained at 8.5 (A and B) and 30 (C and D) μM Ca_i²⁺ from a single *dSlo* channel. The lines are maximum likelihood fits with sums of exponentials. The distributions are normalized to 100,000 intervals for ease of comparison. The open intervals obtained at 8.5 μM Ca_i²⁺ ($P_O = 0.099$; 25,646 fitted intervals) were described by the sum of three significant exponential components with time constants (and areas) of 0.07 ms (0.119), 0.24 ms (0.298), and 0.46 ms (0.583). The open intervals at 30 μM Ca_i²⁺ ($P_O = 0.694$; 68,630 fitted intervals) were also described by the sum of three significant exponential components: 0.04 ms (0.044), 0.18 ms (0.174), and 0.34 ms (0.781). The closed intervals obtained at 8.5 μM Ca_i²⁺ (17,528 fitted intervals) were described by the sum of six significant exponential components: 0.03 ms (0.538), 0.08 ms (0.288), 0.37 ms (0.085), 3.80 ms (0.016), 24.20 ms (0.062), and 71.27 ms (0.011). The closed intervals at 30 μM Ca_i²⁺ (43,043 fitted intervals) were described by the sum of five significant exponential components: 0.03 (0.605), 0.06 ms (0.275), 0.18 ms (0.079), 0.64 ms (0.022), and 1.71 ms (0.019). Channel H06.

in Fig. 6 (three experiments). In contrast, mean closed time decreased in these experiments from ~1 ms at 30 μM Ca_i²⁺ to ~0.1 ms at 3000 μM Ca_i²⁺.

The failure of high Ca_i²⁺ to decrease mean open time suggests that the apparent Ca²⁺-insensitivity of mean open time observed at lower Ca_i²⁺ (Fig. 3 A) was not due to simple open channel block by Ca_i²⁺ masking a Ca²⁺-induced increase. However, as will be considered in later sections, if the open states are blocked differentially by Ca²⁺, then the observation that high Ca_i²⁺ does not decrease mean open time does not rule out more complex types of block by Ca²⁺.

In addition to increasing mean open time, high Ca_i²⁺ (3000 μM) also reduced the single-channel current amplitude by ~10%, as shown in Fig. 6. A reduction in conductance at millimolar Ca_i²⁺ has also been observed for native skeletal muscle BK channels, and is consistent with possible screening effects of Ca²⁺ in the vestibule of the channel (Ferguson, 1991).

2-D dwell-time distributions contain correlation information

To develop kinetic schemes that can account for the single-channel kinetics of gating, it is necessary to determine the

connections (transition pathways) among the various open and closed states. Two-dimensional dwell-time distributions, which plot the relative number of times (frequency) various pairs of adjacent open and closed intervals of specified durations are observed in the single-channel record, contain correlation information that can help determine these connections (Fredkin et al., 1985; Keller et al., 1990; Magleby and Weiss, 1990; Magleby and Song, 1992).

Fig. 7, A and C presents 2-D dwell-time distributions for two different *dSlo* channels. The y and x axes plot the log of the durations of adjacent open and closed intervals in the single-channel record, respectively, and the z axis plots the square root of the number of observations in each bin (see Methods). In theory, the total number of potential peaks in the 2-D dwell-time distribution is equal to the number of kinetic open states multiplied by the number of kinetic closed states, with the peaks located at the intersection of the time constants of the open components on the y axis and the time constants of the closed components on the x axis (Fredkin et al., 1985; Rothberg et al., 1997). Fitting the dwell-time distributions for the channels represented in Fig. 7, A and C gave four open and six closed exponential components, suggesting 24 potential peaks for each channel.

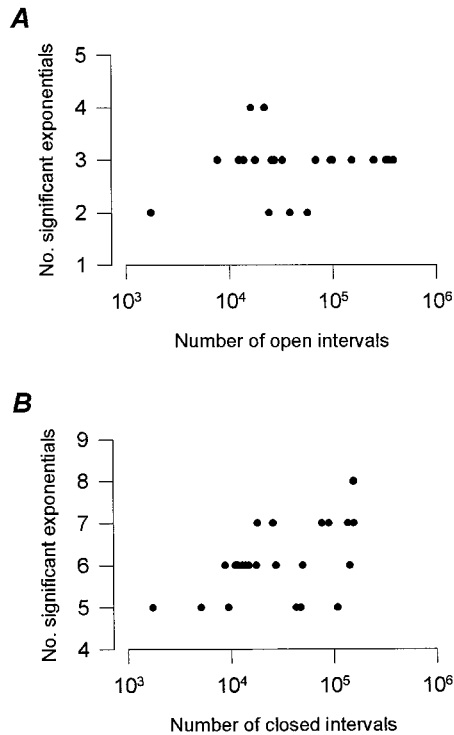


FIGURE 5 The numbers of significant open (A) and closed (B) exponential components are plotted against the number of fitted intervals for 23 open and 23 closed dwell-time distributions from *dSlo*. The 23 pairs of open and closed 1-D dwell-time distributions are from 10 different channels with data obtained at one to five different Ca_i^{2+} for each channel.

In practice, the only visibly distinct peaks in 2-D dwell-time distributions are those arising from components composed of the most frequent interval combinations or those arising from components with time constants widely separated from those of other components (Magleby and Weiss, 1990; Magleby and Song, 1992; Rothberg et al., 1997). For example, for the channels presented in Fig. 7, A and C, it first appears that only two of the potential 24 peaks are visible. However, upon closer inspection, the peaks are wider than would be expected for single exponentials, and slight inflections can be seen on the sides of the peaks, suggesting that each of the two major peaks are composed of a number of underlying 2-D components. The highest peak in Fig. 7, A and C (*peak 4*) arises mainly from long open intervals adjacent to brief closed intervals; this combination occurs most frequently. In contrast, the peak arising from brief open intervals adjacent to long closed intervals (*peak 3*) is considerably lower; this combination occurs less frequently.

Two-dimensional dwell-time distributions were examined for eight additional *dSlo* channels. In general, the major features of the 2-D dwell-time distributions were conserved among all *dSlo* channels examined. (Additional examples of 2-D dwell-time distributions will be presented in a later section.).

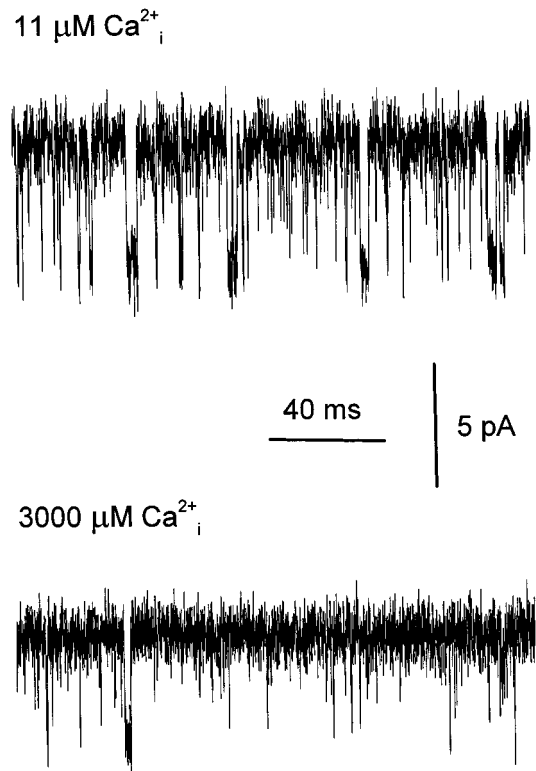


FIGURE 6 Very high Ca_i^{2+} can increase the observed mean open time of *dSlo*. Currents recorded from a single *dSlo* channel at 11 and 3000 $\mu\text{M Ca}_i^{2+}$. Currents were low-pass filtered at 7 kHz. Channel C51.

Dependency plots present information about the kinetic structure of *dSlo* channels

Although 2-D dwell-time distributions contain correlation information, this information is not obvious from visual inspection of the plots because the relative heights of the individual peaks indicate the relative frequency of occurrence of the various pairs of open and closed interval durations, and not whether a given pair is in excess or deficit over what would be expected from random pairing of the intervals. Dependency plots provide a means to display this correlation information (Magleby and Song, 1992). A dependency plot presents the fractional difference between the observed number of adjacent open and closed intervals of indicated durations and the hypothetical number that would be observed if all of the open and closed intervals paired independently (Eqs. 1 and 2 in Methods).

Dependencies of +0.5 or -0.5 would indicate 50% more or 50% fewer observed interval pairs, respectively, than expected for independent pairing of open and closed intervals. Thus, a negative dependency for a given interval pair suggests a relative deficit of effective transition pathways between the open and closed kinetic states (including compound states) that give rise to that pair. Conversely, a positive dependency for an interval pair suggests the presence of effective transition pathways between the open and closed kinetic states (including compound states) that give

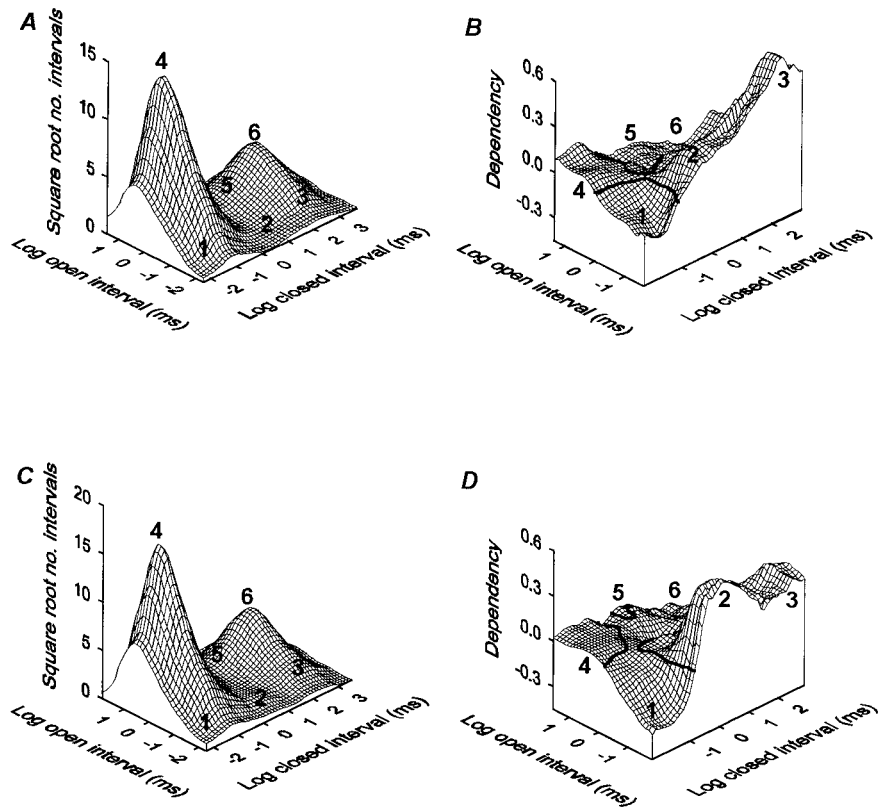


FIGURE 7 Two-dimensional (2-D) dwell-time distributions and dependency plots for two *dSlo* channels. (A and B) 2-D dwell-time distribution (A) and dependency plot (B) for a *dSlo* channel with a P_O of 0.076; $11 \mu\text{M Ca}_i^{2+}$; 33,309 plotted interval pairs. Low-pass filtered at 7 kHz. Dead time = $30 \mu\text{s}$. Channel H23. (C and D) 2-D dwell time distribution (C) and dependency plot (D) for a *dSlo* channel with a P_O of 0.125; $11 \mu\text{M Ca}_i^{2+}$; 46,472 plotted interval pairs. Low-pass filtered at 9 kHz. Dead time = $20 \mu\text{s}$. Channel H21. In this and the following figures the heavy lines in the dependency plots indicate a dependency of zero.

rise to that pair (Magleby and Song, 1992; Rothberg et al., 1997). Because dependency plots present high gain representations of excesses and deficits in the observed number of interval pairs relative to the expected number assuming independent pairing, estimates of dependency can be unreliable where the numbers of observed interval pairs per bin in the 2-D dwell-time distributions are small. Consequently, references to dependency in the following sections will be made only where a sufficient number of interval pairs contribute to the dependencies to obtain reliable estimates (see Rothberg and Magleby, 1998). Such dependencies will be referred to by numbers on the dependency plots.

Fig. 7, B and D presents dependency plots derived from the 2-D distributions in Fig. 7, A and C, respectively. The heavy lines indicate a dependency of zero. These dependency plots share several major features. First, there is a 20–30% deficit of brief open intervals adjacent to brief closed intervals (Fig. 7, B and D, position 1). This deficit suggests a relative lack of effective transitions between the open and closed states giving rise to the brief open intervals and brief closed intervals. Second, there is a 20% deficit of long open intervals adjacent to long closed intervals (Fig. 7, B and D, position 6). This deficit suggests a relative lack of effective transitions between the open and closed states giving rise to the long open intervals and long closed intervals. Third, there is a 30–60% excess of brief open intervals adjacent to long closed intervals (Fig. 7, B and D, position 3). This excess suggests that there is an effective connection between the open and closed states giving rise to

the brief open intervals and the long closed intervals. Finally, there is a 5–10% excess of long open intervals adjacent to brief closed intervals (Fig. 7, B and D, position 4). Although the dependency is small at position 4, this small fractional excess involves a large number of intervals because of the large number of intervals at position 4 in the 2-D dwell-time distributions. The excess at position 4 in the dependency plots suggests that there is an effective connection between the open and closed states giving rise to the long open intervals adjacent to the brief closed intervals.

Dependency plots were examined for eight additional *dSlo* channels. In general, these four prominent excesses and deficits of interval pairs (positions 1, 3, 4, and 6) were observed in dependency plots obtained from all *dSlo* channels analyzed with 2-D methods.

In addition to these major features, the plots also suggested that the dependency of brief open intervals (<0.1 ms) adjacent to intermediate closed intervals (~ 1 ms) increased as P_O increased. To investigate this possibility, we plotted the dependency at position 2 against P_O for 16 dependency plots obtained from nine *dSlo* channels over a range of Ca_i^{2+} (Fig. 8). Although there was variability in response, the dependency at position 2 did increase as a function of P_O . Data from channels H23 and H21 (*open circle* and *open square* in Fig. 8) were selected for presentation in Fig. 7 because these data gave two representative examples of the types of responses that could be observed, and also because these data had large numbers of intervals,

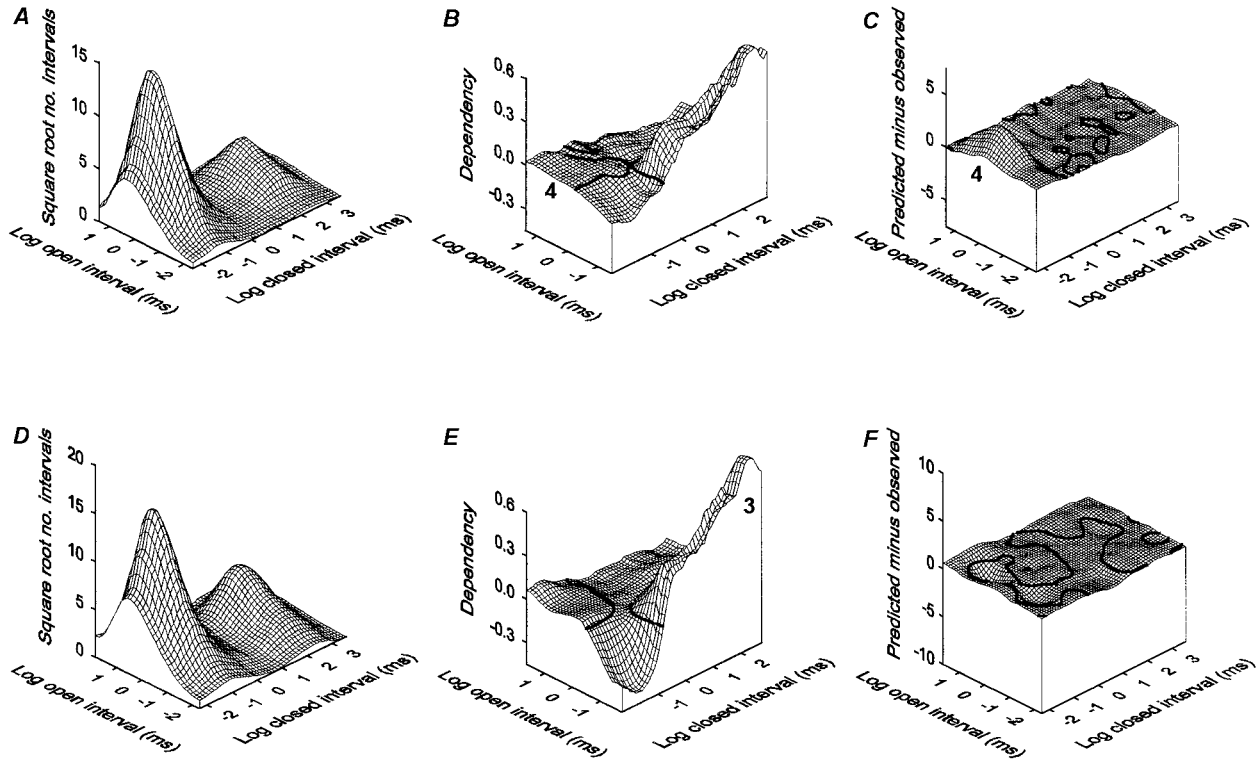


FIGURE 9 Two-dimensional (2-D) dwell-time distributions and dependency plots predicted by Scheme 1. (A and B) Predicted 2-D dwell-time distribution and dependency plot for channel H23. Predicted $P_O = 0.090$; $11 \mu\text{M Ca}_i^{2+}$; 33,300 plotted interval pairs. Dead time = $30 \mu\text{s}$. (D and E) Predicted 2-D dwell-time distribution and dependency plot for channel H21. Predicted $P_O = 0.116$; $11 \mu\text{M Ca}_i^{2+}$; 47,000 plotted interval pairs. Dead time = $20 \mu\text{s}$. (C and F) Difference plots of the predicted 2-D dwell-time distributions minus the observed 2-D dwell-time distributions (Fig. 9 A minus Fig. 7 A in C, and Fig. 9 D minus Fig. 7 C in F). The difference plots are the square root of the numbers of predicted intervals minus the square root of the numbers of observed intervals. Rate constants (s^{-1}): 1–2 = 1239 (H23), 1202 (H21); 2–3 < 0.1, < 0.1; 4–5 = 13483, 11568; 5–6 = 1902, 2914; 6–7 = 1954, 1616; 7–8 = 0.40, 0.15; 6–3 = 203, 44.9; 3–6 = 8911, 16491; 5–2 = 31950, 24439; 2–5 = 3344, 725; 4–1 < 0.1, < 0.1; 1–4 < 0.1, < 0.1. Ca²⁺-dependent rate constants ($\mu\text{M}^{-1} \text{s}^{-1}$): 2–1 = 63.0, 85.1; 3–2 < 0.1, < 0.1; 5–4 = 387, 359; 6–5 = 107, 47.0; 7–6 = 1.1, 1.9; 8–7 = 0.20, 0.17.

likelihood ratios normalized to 1000 pairs of intervals, NLR_{1000} , were calculated (see Eq. 3 in Methods). A NLR_{1000} of 1.0 would indicate that a kinetic scheme describes the distributions as well as theoretically possible for a discrete-state Markov model with the same number of states as in the kinetic scheme. When the 2-D dwell-time distributions obtained at a single Ca_i^{2+} from nine *dSlo* channels were fitted with Scheme 1, the NLR_{1000} ranged from 0.00024 to 0.059. In contrast, when the same 2-D distributions were fitted with Scheme 2, the NLR_{1000} ranged from 0.24 to 0.60, indicating that Scheme 2 provided a better description of the data. (The log likelihood ratio (LLR), given by the log likelihood for Scheme 2 minus the log likelihood for Scheme 1, ranged from 75 to 176 for the examined channels, also indicating that Scheme 2 gave a better description of the data than Scheme 1.) While the NLR_{1000} gives a measure of how well a given model describes the data, it cannot be used for ranking schemes, since no penalty is applied for the number of free parameters. To overcome this difficulty, the Schwarz criterion was used to apply penalties and rank models (Eq. 4 in Methods). Using the Schwarz criterion, Scheme 2 ranked above Scheme 1 for all *dSlo* channels studied at a single Ca_i^{2+} . For

example, for channel H21 (Fig. 7, C and D) the Schwarz criterion was 124,561 for Scheme 2 and 124,707 for Scheme 1, where the scheme with the smallest value ranks first (see Methods). Thus, the visual impressions from the kinetic structure suggesting that Scheme 2 describes the data better than Scheme 1 are in agreement with the quantitative rankings.

Fig. 11 presents five sets of rate constants for Scheme 2 obtained by fitting five different *dSlo* channels. The top two bars in each set of five are for the two representative *dSlo* channels in Fig. 7 fitted at a single Ca_i^{2+} . (The bottom three bars are for simultaneous fitting of data obtained at different Ca_i^{2+} and will be discussed later.) In general, the relative values of the rate constants for Scheme 2, in terms of which were fast and which were slow, were similar for the nine different channels fitted at a single Ca_i^{2+} . However, there could be large differences in estimates of some of the rate constants, such as for rates 2–3 and 3–2, which are in a loop and were typically poorly defined. For most channels, the closing rates from states C_9 , C_{10} , and C_{11} were typically fast so that the mean lifetimes of these states were very brief (~ 0.05 ms). Each channel was also fitted with a version of Scheme 2 in which the closing rates for states C_9 , C_{10} , and C_{11} were constrained so that these states would have identical mean

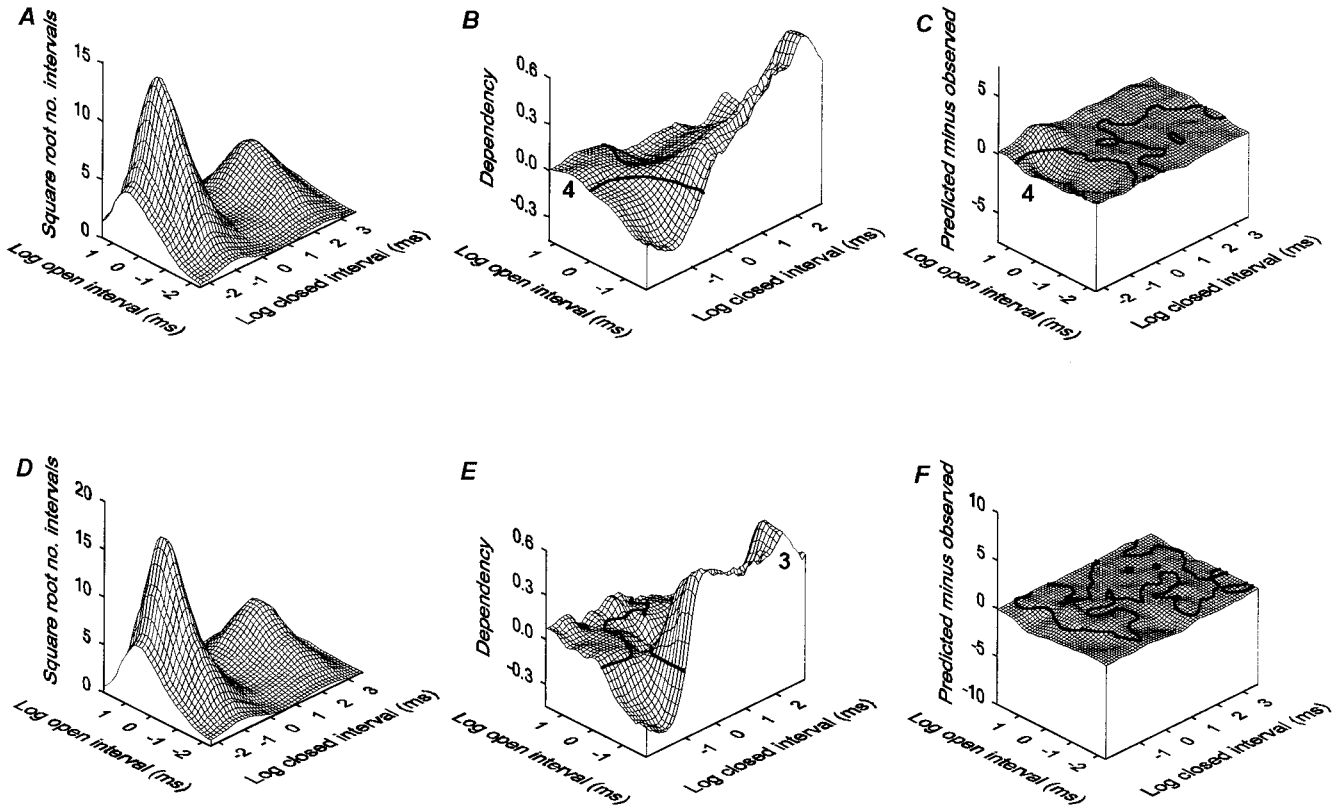
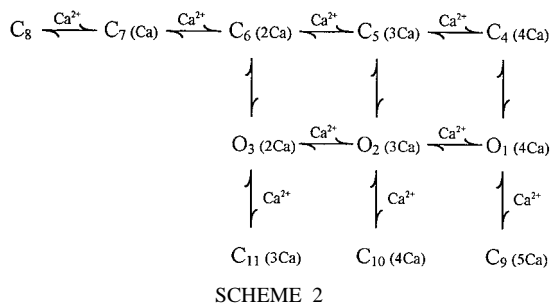


FIGURE 10 Two-dimensional (2-D) dwell-time distributions and dependency plots predicted by Scheme 2. (A and B) Predicted 2-D dwell-time distribution and dependency plot for channel H23. Predicted $P_O = 0.079$; $11 \mu\text{M Ca}_i^{2+}$; 33,500 plotted interval pairs. Dead time = $30 \mu\text{s}$. (D and E) Predicted 2-D dwell-time distribution and dependency plot for channel H21. Predicted $P_O = 0.122$; $11 \mu\text{M Ca}_i^{2+}$; 47,000 plotted interval pairs. Dead time = $20 \mu\text{s}$. (C and F) Difference plots of the predicted 2-D dwell-time distributions minus the observed 2-D dwell-time distributions (Fig. 10 A minus Fig. 7 A in C, and Fig. 10 D minus Fig. 7 C in F). The rate constants are presented in Fig. 11.



lifetimes. In most cases, constraining the closing rates in this manner had little effect on the results for fitting data at a single Ca_i^{2+} .

Scheme 2 approximates the effects of changing Ca_i^{2+} on *dSlo* gating kinetics

While Scheme 2 provides a reasonable description of the kinetic structure at a single Ca_i^{2+} , a further test would be to see how well the model can account for the effects of changes in Ca_i^{2+} on *dSlo* gating kinetics, as revealed by the kinetic structure. Fig. 12 presents 2-D dwell-time distributions and dependency plots for a representative *dSlo* channel

(channel H06) at three different Ca_i^{2+} . Note the pronounced shift of long closed intervals to briefer durations as Ca_i^{2+} was increased, as indicated by the leftward shift of the arrows in Fig. 12, A, C, and E, where the arrows indicate the peaks.

Estimates of the most likely rate constants for Scheme 2 were determined by simultaneously fitting the 2-D dwell-time distributions obtained at three or four different Ca_i^{2+} for each of three different *dSlo* channels. Fig. 13 presents the 2-D dwell-time distributions, dependency plots, and difference plots predicted by Scheme 2 at 8.5, 11, and $30 \mu\text{M Ca}_i^{2+}$ for the channel shown in Fig. 12. Comparison of Figs. 12 and 13 indicates that Scheme 2 accounted for the major features of the Ca^{2+} -dependent shifts in the 2-D dwell-time distributions, including the shift from longer to briefer closed interval durations. (The arrows are from Fig. 12 and indicate where the peaks of the observed distributions would fall.) Scheme 2 also approximated the basic features of the Ca^{2+} -dependent shifts of the dependency plots, but with some differences. For example, Scheme 2 underpredicted position 3 for $11 \mu\text{M Ca}_i^{2+}$. However, the difference plots indicate that the errors were small, especially at $30 \mu\text{M Ca}_i^{2+}$. A similar ability to approximate the dwell-time distributions and dependency plots was obtained for each of the other two channels analyzed in this manner.

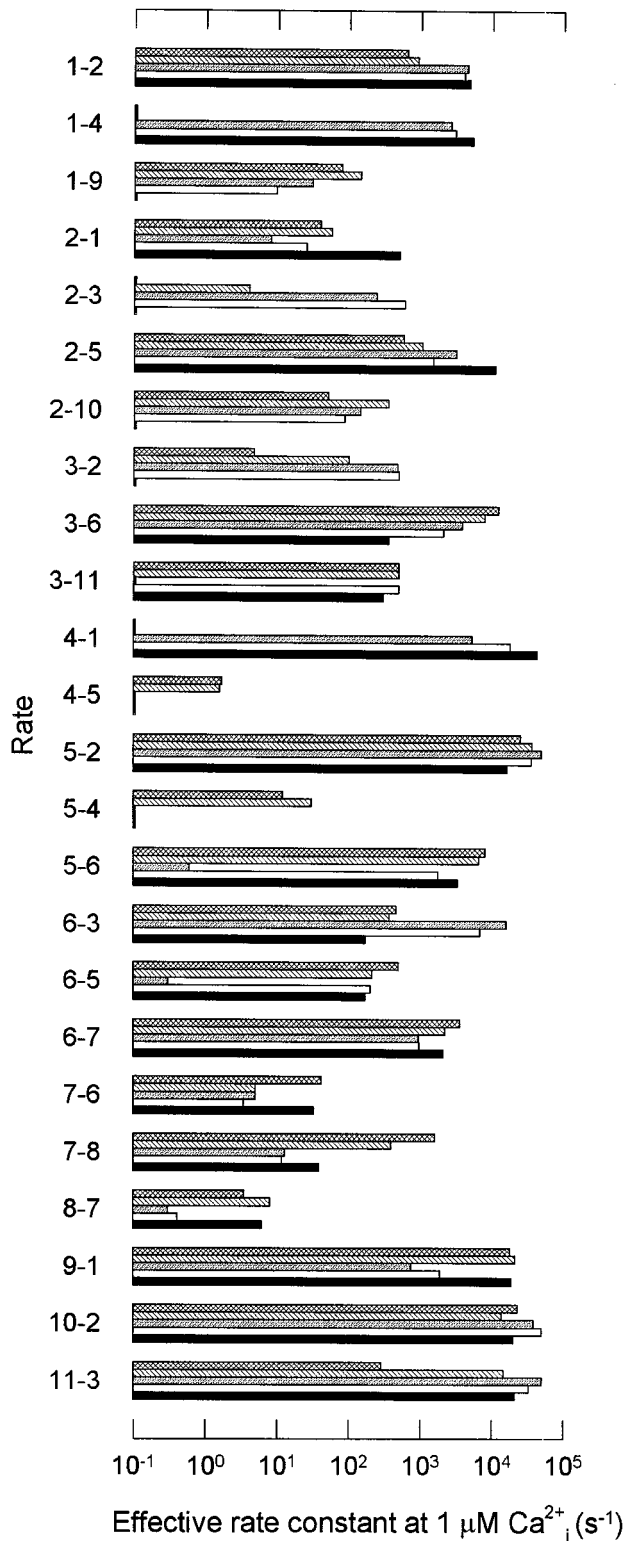


FIGURE 11 Estimated rate constants for Scheme 2. Estimates are presented for two channels fitted at a single Ca_i²⁺ (H21, criss-crossed bar; H23, cross-hatched bar), one channel fitted at four different Ca_i²⁺ (H08, light gray bar), and two channels fitted at three different Ca_i²⁺ (H10, white bar; H06, black bar). The bars at 10⁻¹ μM⁻¹ s⁻¹ indicate that the rate constants were this value or less.

The dashed lines in Fig. 3, A and B plot the predicted mean open and closed times for Scheme 2 as a function of Ca_i²⁺ for channel H06 and also for the two other channels analyzed by simultaneous fitting of 2-D dwell-time distributions obtained at different Ca_i²⁺. The mean open times are well-described for the fitted channels, and the Ca_i²⁺ dependence of the mean closed times are reasonably described for two of the three fitted channels. For the third channel (*squares*) the observed decrease in mean closed time was somewhat greater than predicted.

Although gating was not studied in detail at high Ca_i²⁺, the predicted response of Scheme 2 at high Ca_i²⁺ for channel H06 was calculated. Increasing Ca_i²⁺ from 11 μM to 3000 μM increased the predicted mean open time 2-fold and decreased mean closed time ~30-fold (not shown), which is consistent with the observations made at high Ca_i²⁺. Thus, Scheme 2 can predict a dual response in plots of mean open time versus Ca_i²⁺ (little or no effect for low to moderate Ca_i²⁺ followed by an increasing mean open time for high Ca_i²⁺), and a monotonic decrease in mean closed time. In terms of Scheme 2, the dual response in mean open time for channel H06 arose because the Ca²⁺-dependent rate constants for transitions O₁-C₉ and O₂-C₁₀ were considerably less than for transition O₃-C₁₁. Thus, as higher Ca_i²⁺ drives the gating away from O₃ and O₂ toward O₁, the effective rate of transitions to the brief closed states is decreased, leading to longer mean open intervals.

The NLR₁₀₀₀ for Scheme 2 for the three channels, each fitted simultaneously to three or four different Ca_i²⁺, ranged from 3.4 × 10⁻³ to 1.3 × 10⁻¹² (Table 1). Thus, the NLR₁ for a single interval pair (given by (NLR₁₀₀₀)^{0.001}) ranged from 0.994 to 0.973, suggesting an average likelihood difference per interval pair of 0.6% to 2.7% between the theoretical best fit of the distributions and the descriptions by Scheme 2. This small difference in the normalized likelihood ratio per interval pair is reflected in the ability of Scheme 2 to give reasonable descriptions of the distributions. (A detailed discussion of normalized likelihood ratios can be found in McManus and Magleby, 1991.)

As shown in Table 1, Scheme 2 ranked significantly above Scheme 1 (*P* < 0.001) for all three channels that were each fitted simultaneously to three or more Ca_i²⁺. The consistent finding that Scheme 2 ranked above Scheme 1, whether fitting data obtained at a single Ca_i²⁺ or multiple Ca_i²⁺, reduces the possibility that the ranking was affected by possible drift in the data that would be more likely to occur when data are collected over a range of Ca_i²⁺. A further reason for rejecting Scheme 1 is that the dependency plots predicted for Scheme 1 with rate constants obtained by simultaneous fitting of multiple Ca_i²⁺ did not predict (not shown) the inverse relationship between the durations of adjacent open and closed intervals that is consistently observed in the dependency plots in the experimental data (notice in Figs. 7 and 12 that brief closed intervals tend to be adjacent to long open intervals and long closed intervals tend to be adjacent to brief open intervals).

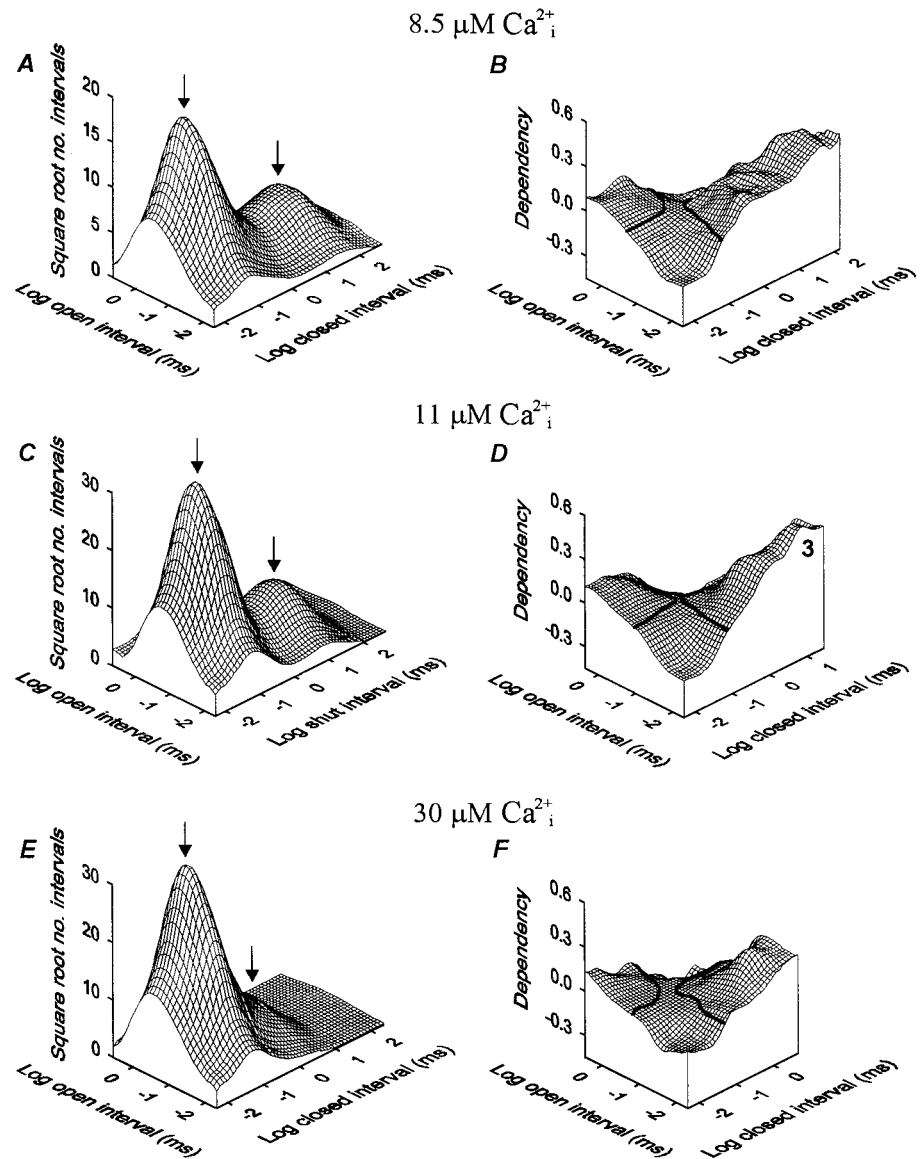


FIGURE 12 Changes in kinetic structure with increasing Ca_i^{2+} . 2-D dwell-time distributions and dependency plots for channel H06 at three different Ca_i^{2+} . (A and B) $P_O = 0.10$; 56,751 interval pairs. (C and D) $P_O = 0.18$; 159,147 interval pairs. (E and F) $P_O = 0.69$; 151,915 interval pairs. The arrows indicate the positions of the two prominent peaks in the dwell-time distributions. Dead time = 20 μs .

The rate constants obtained for Scheme 2 for channel H06 and the two additional channels included in Table 1 are presented in Fig. 11 (lower three bars for each rate). For the three channels fitted at multiple Ca_i^{2+} , there were very rapid transitions between states O_1 and C_4 , whereas there were very few transitions between these two states for the channels fitted at a single Ca_i^{2+} . Such a difference may reflect that the rate constants between O_1 and C_4 are poorly defined or may reflect the greater restrictions on rate constants imposed by fitting multiple Ca_i^{2+} . To distinguish among these possibilities, each channel fitted at a single Ca_i^{2+} was also fitted with Scheme 2, in which the rate constants between O_1 and C_4 were constrained to those values obtained from channels fitted at multiple Ca_i^{2+} . In each case the constrained model for the single data sets ranked significantly below the unconstrained one (not shown). Consequently, the rate constants between O_1 and C_4 are well defined, and the large differences in the values of these rate

constants when fitting single and multiple data sets most likely reflect that Scheme 2 is simpler than the actual gating mechanism. If the scheme were correct and the data perfect, then the rate constants obtained from the simultaneous fitting of multiple data sets should also describe the single data sets as well as when fitting single data sets alone.

Schemes 3 and 4 ranked below Scheme 2

In contrast to the Ca^{2+} -dependent transitions to the brief closed intervals in Scheme 2, Rothberg and Magleby (1998) found that Scheme 3, in which the transitions to the brief closed intervals were not Ca^{2+} -dependent, gave improved descriptions of the kinetic structure of native BK channels in rat skeletal muscle when compared to Scheme 1. Consequently, we examined how well Scheme 3 could account for the Ca^{2+} -dependent kinetics of *dSlo*. As shown in Table 1, Scheme 3 ranked above Scheme 1, but below Scheme 2.

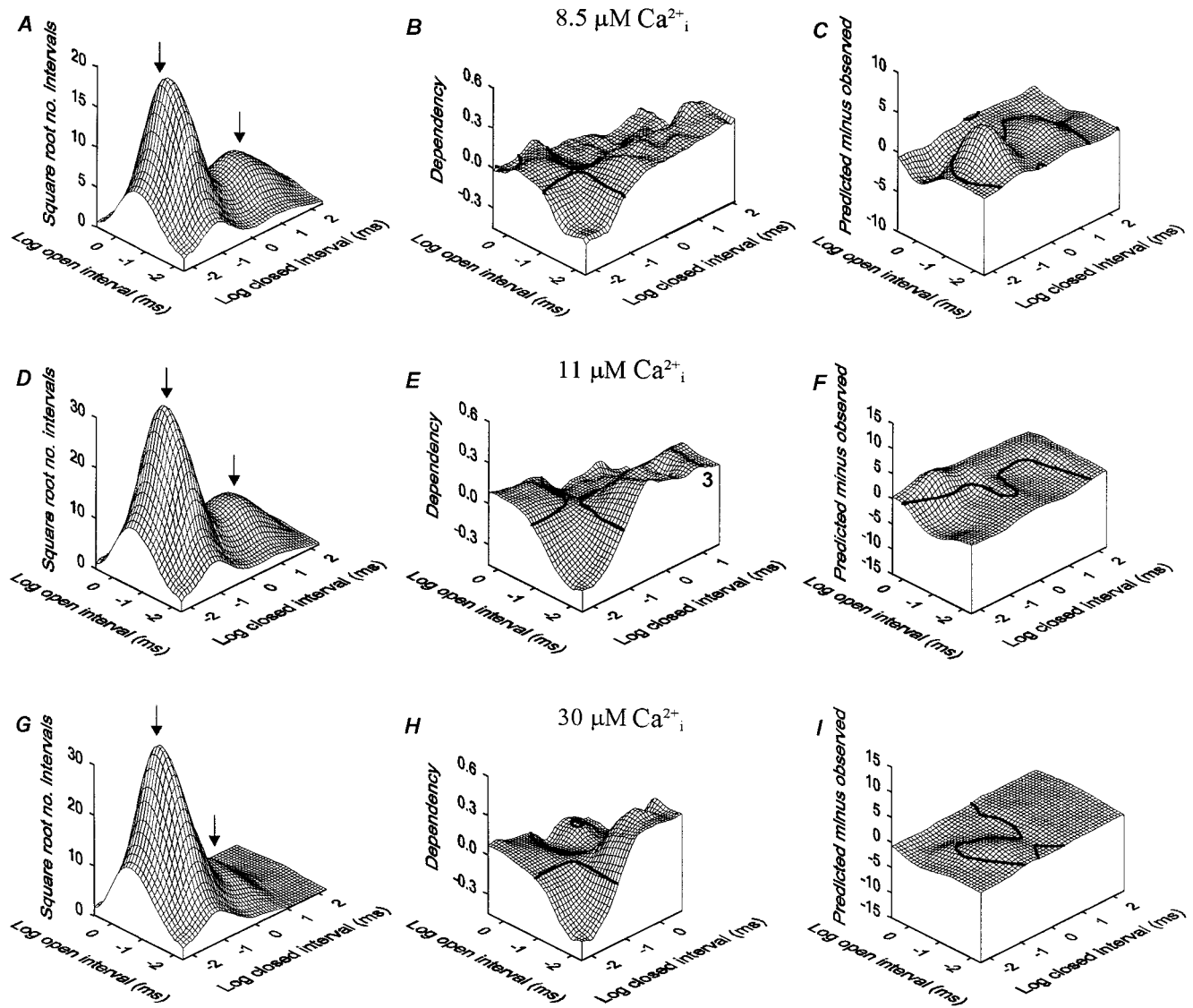


FIGURE 13 Scheme 2 approximates the kinetic structure of *dSlo*. Two-dimensional dwell-time distributions and dependency plots predicted by Scheme 2 for channel H06. Compare to the observed kinetic structure in Fig. 12. The arrows are from Fig. 12 and indicate where the peaks of the observed distributions would fall. (A–C) Predicted $P_O = 0.10$. (D–F) Predicted $P_O = 0.17$. (G–I) Predicted $P_O = 0.62$. (C, F, and I) Difference plots of the predicted 2-D dwell-time distributions minus the observed 2-D dwell-time distributions in Fig. 12. Dead time = 20 μ s. The rate constants are in Fig. 11.

DiChiara and Reinhart (1995) have suggested that the gating of *dSlo* is consistent with Scheme 4, which has only the first two Ca²⁺-binding sites when compared to the four Ca²⁺-binding sites of Scheme 1. For the three channels examined with simultaneous fitting in our study, Scheme 4 ranked lower than Schemes 1–3 (Table 1).

More complex schemes

In addition to Schemes 1–4, a number of more complex schemes with additional states and/or different connections among the states were examined. In general, the large numbers of free parameters in these more complex models resulted in many of the rate constants being poorly defined, and it was also difficult to determine whether the most

likely rate constants had been found for such complex models. Consequently, examination of more complex models is best delayed until additional data, such as channel activity over a range of voltages and a wider range of Ca²⁺_i, and also from step changes in Ca²⁺_i, are obtained to better define and constrain the rate constants.

DISCUSSION

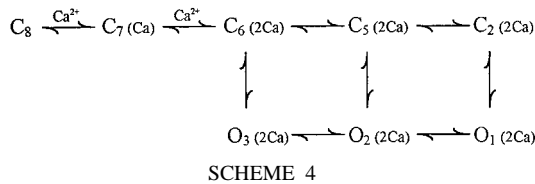
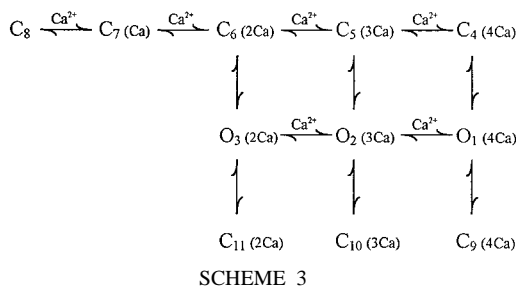
The results of this study suggest that the effects of increasing Ca²⁺_i on the gating kinetics of *dSlo* variant A1/C2/E1/G3/IO are complex and can be divided into at least two phases. Increasing Ca²⁺_i from 5 to 30 μ M had little effect on mean open time, whereas increasing Ca²⁺_i to high concentrations (300–3000 μ M) typically increased mean open

TABLE 1 Log-likelihood ratios (LLR), normalized likelihood ratios (NLR₁₀₀₀), and rankings (R) of schemes 1–4

Scheme	Channel H08			Channel H10			Channel H06		
	LLR	NLR ₁₀₀₀	R	LLR	NLR ₁₀₀₀	R	LLR	NLR ₁₀₀₀	R
4	14,174	2.7×10^{-14}	4	5778	6.8×10^{-13}	4	4586	9.7×10^{-21}	4
1	999	6.1×10^{-4}	3	2603	9.3×10^{-9}	3	904	4.1×10^{-14}	3
3	910	6.5×10^{-4}	2	150	1.2×10^{-5}	2	682	7.9×10^{-14}	2
2*	0	3.4×10^{-3}	1	0	1.9×10^{-5}	1	0	1.3×10^{-12}	1

Each channel was fitted simultaneously at three (H10 and H06) or four (H08) different Ca_i^{2+} . LLR is calculated from the log-likelihood for scheme 2 minus the log-likelihood for the indicated scheme. NLR₁₀₀₀ (Eq. 3 in Methods) is the ratio of the likelihood of the indicated scheme to the likelihood of the theoretical best fit to the distributions determined with sums of exponentials. The NLR₁₀₀₀ is normalized to what would be observed for 1000 interval pairs. The rankings are based on the Schwarz criterion, which applies a penalty for additional free parameters (Eq. 4 in Methods).

*The likelihood ratio test (examples in McManus and Magleby, 1988) indicated that Scheme 2 gave a significantly better description of the data than the other schemes ($P < 0.001$). Number of fitted interval pairs: channel H08 = 550,395; channel H10 = 333,328; channel H06 = 241,527.



time. Evaluation of kinetic schemes fit to 2-D dwell-time distributions indicated that previously described schemes that largely account for the Ca^{2+} -dependent kinetics of native BK channels from rat skeletal muscle (Schemes 1 and 3) did not adequately describe the Ca^{2+} dependence of this *dSlo* channel. However, an expanded version of these schemes that permits a Ca^{2+} -facilitated transition from each open state to a brief (secondary) closed state (Scheme 2) could approximate the Ca^{2+} -dependent kinetics of this *dSlo* BK channel variant.

Scheme 2 was the minimal model that described the major features of the Ca^{2+} -dependent gating of *dSlo*. The improvement in the dependency plots predicted by Scheme 2 upon addition of a brief closed state to each open state is similar to results for native BK channels from rat skeletal muscle (Rothberg and Magleby, 1998), suggesting that additional brief closed states may contribute to channel gating. However, for rat skeletal muscle BK channels, transitions to secondary brief closed states are not facilitated by Ca^{2+} , and there is no evidence for discrete Ca^{2+} block in skeletal muscle BK channels (Rothberg et al., 1996).

For *dSlo* and Scheme 2, the relative occupancy of the three open states shifts with increasing Ca_i^{2+} , and the rate constants for the Ca^{2+} -facilitated transitions to the brief

(secondary) closed states can differ for different open states. It is this combination of Ca^{2+} -dependent shifting and Ca^{2+} -facilitated blocking that allows Scheme 2 to provide a two-phase response in mean open time with increasing Ca_i^{2+} for *dSlo*. (Note that the Ca^{2+} -facilitated blocking for *dSlo* in Scheme 2 is derived solely from kinetic modeling, without direct evidence for such block. Hence, Scheme 2 must be considered only a working hypothesis.)

Ca^{2+} -dependent transitions to secondary closed states have been proposed previously by Wu et al. (1995) for BK channels in turtle cochlear hair cells to account for an observed shift from briefer to longer duration closed intervals at the highest Ca_i^{2+} examined (35 μM). The model of Wu et al. (1995) is the same as Scheme 2, except that state C_{11} is omitted in their model. In addition, the lifetimes of the Ca^{2+} -induced secondary closed states obtained by Wu et al. (1995) differ from those obtained with Scheme 2 for fitting *dSlo*. The lifetimes of the secondary closed states for the cochlear BK channels are 1.7 ms and 12.5 ms, compared to ~ 0.05 ms for *dSlo*. Thus, the effective gating mechanisms for *dSlo*, native BK channels from rat skeletal muscle, and native BK channels from turtle cochlear hair cells appear to have some differences.

The effects of Ca_i^{2+} on kinetics can differ among *dSlo* channels

From Fig. 3, A and B it can be seen that there is variability among channels in the plots of mean open and closed time versus Ca_i^{2+} , with the greatest variability for the closed times. Variability in the properties of cloned channels expressed in *Xenopus* oocytes has also been observed for the Ca^{2+} sensitivity of *dSlo* channels (Silberberg et al., 1996), the time course of inactivation of *Shaker* K^+ channels (Ciorba et al., 1997), and the kinetics of nicotinic acetylcholine receptors (Gibb et al., 1990). The mechanism underlying the variable Ca^{2+} -dependent kinetics of *dSlo* is not known, but could be related to differences in the environment of the channels or to chemical modification of the subunits of the channels. For example, the activity of BK channels in rat neuroepithelium and rat brain BK channels reconstituted in planar lipid bilayers can be altered by

cytoskeletal proteins (Mienville et al., 1996; Kitzmiller and Rosenberg, 1997), and BK channels can be modulated by posttranslational modifications such as phosphorylation (Reinhart et al., 1991; Bielefeldt and Jackson, 1994) and oxidation/reduction (DiChiara and Reinhart, 1997; Thuringer and Findlay, 1997).

While one or more of the factors considered above may have contributed to the variable response among channels in the observed mean open and closed times in this study, it cannot be ruled out that some form of mode shifting (McManus and Magleby, 1988) occurred at the time of the solution changes (so that it was not detected). This seems less likely, however. The observed changes in activity with changes in Ca_i²⁺ did not appear consistent with the known mode shifts for BK channels (McManus and Magleby, 1988).

Comparison to previous studies

Lagrutta et al. (1994) and DiChiara and Reinhart (1995) observed that the mean open time of *dSlo* is relatively Ca²⁺-insensitive for Ca_i²⁺ < 75 μM. Our observations are in agreement with theirs and also suggest that the mean open time of *dSlo* channels becomes Ca²⁺-sensitive when Ca_i²⁺ is increased to very high concentrations (300–3000 μM). The Ca²⁺-dependent kinetics of *dSlo* differ markedly from those of native BK channels from cultured rat skeletal muscle. For BK channels from rat muscle, mean open time increased consistently and dramatically over the entire range of examined Ca_i²⁺ (1–23 μM, Fig. 3 C) and can increase further as Ca_i²⁺ is increased to millimolar concentrations (B. S. Rothberg and K. L. Magleby, unpublished observations).

In terms of Schemes 1 and 3, this increase for the native skeletal muscle BK channel arises because increasing Ca_i²⁺ drives the gating toward the longer lifetime open states (O₂ and O₃). In terms of Scheme 2 for *dSlo*, the increase does not occur at lower Ca_i²⁺ because of Ca²⁺-facilitated brief closings. Despite these differences in Ca²⁺-dependent kinetics, the basic features of the dependency plots for *dSlo* in the present study appear similar to those for native BK channels in skeletal muscle presented in Rothberg and Magleby (1998). Each channel type shows an inverse relationship between the duration of adjacent open and closed intervals, such that brief open intervals tend to be adjacent to long closed intervals and long open intervals tend to be adjacent to brief closed intervals. This suggests that *dSlo* and rat skeletal muscle BK channels may share some fundamental similarities in gating mechanism.

Other types of Ca²⁺-activated K⁺ channels may have Ca²⁺-dependent kinetics similar to *dSlo*. The mean open times of small conductance Ca²⁺-activated K⁺ channels are independent of intracellular Ca_i²⁺ (Hirschberg et al., 1998), and the mean open times of BK channels purified from bovine aortic smooth muscle also show no apparent Ca²⁺ dependence (Giangiacomo et al., 1995). Whether this lack

of Ca²⁺ dependence for smooth muscle reflects a similarity in gating to *dSlo* channels or results from the limited frequency response of recordings from bilayers is not yet clear.

Possible mechanisms for Scheme 2

Because the Ca²⁺-facilitated transitions to brief closed states in Scheme 2 include both Ca²⁺ binding and the transition to a nonconducting state in a single step, this model suggests that the observed insensitivity of mean open time to increasing Ca_i²⁺ (<30 μM) may occur directly through discrete Ca²⁺-block of the channel. A discrete Ca²⁺-block mechanism has also been proposed for BK channels in plant vacuoles to account for an increase in the frequency of intermediate closed intervals with increasing Ca_i²⁺ (Laver, 1992). This type of discrete Ca²⁺ block is distinct from the graded reduction in conductance observed at millimolar Ca_i²⁺ (Fig. 6) which may be due to the screening of negative charges by Ca²⁺ and displacement of K⁺ from the inner vestibule of the channel (Ferguson, 1991). It should be noted that Scheme 2 differs from the activation/blockade model of Methfessel and Boheim (1982). In their model, Ca²⁺ facilitates unblocking of the channel rather than blocking, as in Scheme 2. Scheme 2 also differs from the Ca²⁺-dependent inactivation model of Hicks and Marrion (1998) in which inactivation involves large reductions in P_o.

Although Scheme 2 is drawn as a discrete Ca²⁺ block model (for simplicity), our results are also consistent with a mechanism in which the observed insensitivity of mean open time to increasing Ca_i²⁺ could occur indirectly through a Ca²⁺-induced allosteric effect. In this case, the three brief secondary closed states in Scheme 2 (C₉–C₁₁) would each be converted into two states: an initial open state with an additional bound Ca²⁺ followed by a transition to a brief secondary closed state. If this were the case, then Ca²⁺ binding to the channel would induce at least two general types of conformational changes: those that activate the channel and those that generate brief closed intervals through sojourns to secondary closed states.

An allosteric model in which Ca²⁺ exerts dual effects on gating implies at least two different types of Ca²⁺ binding sites at the intracellular surface of the channel. Examination of the deduced primary structure of *dSlo* indicates that the C-terminus contains a string of aspartate residues (“calcium bowl”), mutations of which alter the Ca²⁺ activation of *mSlo* (Schreiber and Salkoff, 1997). In addition, the data of Schreiber and Salkoff (1997) suggest that there may be a second Ca²⁺ binding site involved with activation on each subunit. Unlike *mSlo* (Butler et al., 1993), the C-terminus of *dSlo* also contains a putative Ca²⁺ binding domain suggestive of an EF hand (Atkinson et al., 1991; Adelman et al., 1992), but deletion of this site did not produce obvious changes on the properties of the channel (Adelman et al., 1992).

As pointed out by Eigen (1968), McManus and Magleby (1991), and Cox et al. (1997), tetrameric allosteric proteins

might be expected to enter large numbers of states. For example, a generalized model for allosteric binding to a four subunit protein can lead to 55 states (Cox et al., 1997), most of which would be intermediate between the initial binding steps and full activation. Thus, it is perhaps surprising that such a simple model as Scheme 2 can account for the major features of the Ca^{2+} -dependent gating of *dSlo*, as reflected in 2-D dwell-time distributions and dependency plots (the kinetic structure). It can be difficult to distinguish secondary closed states from the intermediate closed states predicted by allosteric mechanisms (Hoshi et al., 1994; Rothberg and Magleby, 1998). Consequently, some of the brief closed intervals that are generated by the secondary states in Scheme 2 may arise, instead, from intermediate closed states. It is also possible that other simple models that were not tested might describe the gating as well as or better than Scheme 2. Nevertheless, Scheme 2 can serve as a starting point for more detailed studies of the gating of *dSlo*, including its voltage dependence, as well as for other types of Ca^{2+} -activated K^+ channels that display similar gating properties.

The *dSlo* cDNA was a generous gift from J. Adelman. We thank G. Dahl for assistance with the preparation of *Xenopus* oocytes. R. Bello and B. Rothberg provided programs used for 2-D Q-matrix fitting, and the data for native BK channels was from experiments of B. Rothberg and O. McManus.

This work was supported by National Institutes of Health Grants AR32805, NS30584, and NS007044, and a grant from the Muscular Dystrophy Association (to K.L.M.); and the US-Israel Binational Science Foundation Grant 93-00061 and the Israeli Ministry of Science and the Arts Grant 6247194 (to S.D.S.).

REFERENCES

- Adelman, J. P., K. Z. Shen, M. P. Kavanaugh, R. A. Warren, Y. N. Wu, A. Lagrutta, C. T. Bond, and R. A. North. 1992. Calcium-activated potassium channels expressed from cloned complementary DNAs. *Neuron*. 9:209–216.
- Atkinson, N. S., G. A. Robertson, and B. Ganetzky. 1991. A component of calcium-activated potassium channels encoded by the *Drosophila slo* locus. *Science*. 253:551–555.
- Bielefeldt, K., and M. B. Jackson. 1994. Phosphorylation and dephosphorylation modulated a Ca^{2+} -activated K^+ channel in rat peptidergic nerve terminals. *J. Physiol. (Lond.)*. 475:241–254.
- Blatz, A. L., and K. L. Magleby. 1986. Quantitative description of three modes of activity of fast chloride channels from rat skeletal muscle. *J. Physiol. (Lond.)*. 378:141–174.
- Bowlby, M. R., and I. B. Levitan. 1996. Kinetic variability and modulation of *dSlo*, a cloned calcium-dependent potassium channel. *Neuropharmacology*. 35:867–875.
- Butler, A., S. Tsunoda, D. P. McCobb, A. Wei, and L. Salkoff. 1993. *mSlo*, a complex mouse gene encoding “maxi” calcium-activated potassium channels. *Science*. 261:221–224.
- Ciorba, M. A., S. H. Heinemann, H. Weissbach, N. Brot, and T. Hoshi. 1997. Modulation of potassium channel function by methionine oxidation and reduction. *Proc. Natl. Acad. Sci. USA*. 94:9932–9937.
- Colquhoun, D., and A. G. Hawkes. 1981. On the stochastic properties of single ion channels. *Proc. R. Soc. Lond. B*. 211:205–235.
- Colquhoun, D., and F. J. Sigworth. 1995. Fitting and statistical analysis of single-channel records. In *Single-Channel Recording*. B. Sakmann and E. Neher, editors. Plenum Press, New York. 483–587.
- Cox, D. H., J. Cui, and R. W. Aldrich. 1997. Allosteric gating of a large-conductance Ca^{2+} -activated K^+ channel. *J. Gen. Physiol.* 110:257–281.
- Crouzy, S. C., and F. J. Sigworth. 1990. Yet another approach to the dwell-time omission problem of single-channel analysis. *Biophys. J.* 58:731–743.
- Dahl, G. 1992. The oocyte cell-cell channel assay for functional analysis of gap junction proteins. In *Cell-Cell Interactions: A Practical Approach*. B. Stevenson, D. Paul, and W. Gallin, editors. Oxford University Press, London and New York. 143–165.
- DiChiara, T. J., and P. H. Reinhart. 1995. Distinct effects of Ca^{2+} and voltage on the activation and deactivation of cloned Ca^{2+} -activated K^+ channels. *J. Physiol. (Lond.)*. 489:403–418.
- DiChiara, T. J., and P. H. Reinhart. 1997. Redox modulation of *hSlo* Ca^{2+} -activated K^+ channels. *J. Neurosci.* 17:4942–4955.
- Eigen, M. 1968. New looks and outlooks on physical enzymology. *Q. Rev. Biophys.* 1:3–33.
- Esguerra, M., J. Wang, C. D. Foster, J. P. Adelman, R. A. North, and I. B. Levitan. 1994. Cloned Ca^{2+} -dependent K^+ channel modulated by a functionally associated protein kinase. *Nature*. 369:563–565.
- Ferguson, W. B. 1991. Competitive Mg^{2+} block of a large-conductance, Ca^{2+} -activated K^+ channel in rat skeletal muscle. *J. Gen. Physiol.* 98:163–181.
- Fredkin, D. R., M. Montal, and J. A. Rice. 1985. Identification of aggregated Markovian models: application to the nicotinic acetylcholine receptor. In *Proceedings of the Berkeley Conference in Honor of Jerzy Neyman and Jack Kiefer*. L. M. LeCam and R. A. Olshen, editors. Wadsworth Press, Belmont, CA. 269–289.
- Gianguacomo, K. M., M. Garcia-Calvo, H.-G. Knaus, T. J. Mullmann, M. L. Garcia, and O. McManus. 1995. Functional reconstitution of the large-conductance, calcium-activated potassium channel purified from bovine aortic smooth muscle. *Biochemistry*. 34:15849–15862.
- Gibb, A. J., H. Kojima, J. A. Carr, and D. Colquhoun. 1990. Expression of cloned receptor subunits produces multiple receptors. *Proc. R. Soc. Lond. B*. 242:108–112.
- Hamill, O. P., A. Marty, E. Neher, B. Sakmann, and F. J. Sigworth. 1981. Improved patch clamp techniques for high-resolution current recording from cells and cell-free membrane patches. *Pflugers Arch. Eur. J. Physiol.* 391:85–100.
- Hicks, G. A., and N. V. Marrion. 1998. Ca^{2+} -dependent inactivation of large conductance Ca^{2+} -activated K^+ (BK) channels in rat hippocampal neurones produced by pore block from an associated particle. *J. Physiol. (Lond.)*. 508:721–734.
- Hirschberg, B., J. Maylie, J. P. Adelman, and N. V. Marrion. 1998. Gating of recombinant small-conductance Ca^{2+} -activated K^+ channels by calcium. *J. Gen. Physiol.* 111:565–581.
- Hoshi, T., W. N. Zagotta, and R. W. Aldrich. 1994. *Shaker* potassium channel gating I: Transitions near the open state. *J. Gen. Physiol.* 103:249–278.
- Hudspeth, A. J., and R. S. Lewis. 1988. Kinetic analysis of voltage- and ion-dependent conductances in saccular hair cells of the bull-frog, *Rana catesbeiana*. *J. Physiol. (Lond.)*. 400:237–274.
- Keller, B. U., M. S. Montal, R. P. Hartshorne, and M. Montal. 1990. Two-dimensional probability density analysis of single channel currents from reconstituted acetylcholine receptors and sodium channels. *Arch. Biochem. Biophys.* 276:47–54.
- Kitzmler, A., and R. Rosenberg. 1997. Taxol, a stabilizer of microtubules, increases gating instability of Ca^{2+} -activated K^+ channels. *Biophys. J.* 72:20a. (Abstr.).
- Krause, J. D., C. D. Foster, and P. H. Reinhart. 1996. *Xenopus laevis* oocytes contain endogenous large conductance Ca^{2+} -activated K^+ channels. *Neuropharmacology*. 35:1017–1022.
- Lagrutta, A., K. Shen, R. A. North, and J. P. Adelman. 1994. Functional differences among alternatively spliced variants of *slowpoke*, a *Drosophila* calcium-activated potassium channel. *J. Biol. Chem.* 269:20347–20351.
- Latorre, R. 1994. Molecular workings of large conductance (maxi) Ca^{2+} -activated K^+ channels. In *Handbook of Membrane Channels: Molecular and Cellular Physiology*, C. Peracchia, editor. Academic Press, New York. 79–102.

- Laver, D. R. 1992. Divalent cation block and competition between divalent and monovalent cations in the large-conductance K⁺ channel from *Chara australis*. *J. Gen. Physiol.* 100:269–300.
- Magleby, K. L., and L. Song. 1992. Dependency plots suggest the kinetic structure of ion channels. *Proc. R. Soc. Lond. B.* 249:133–142.
- Magleby, K. L., and D. S. Weiss. 1990. Identifying kinetic gating mechanisms for ion channels by using two-dimensional distributions of simulated dwell times. *Proc. R. Soc. Lond. B.* 241:220–228.
- McManus, O. B. 1991. Calcium-activated potassium channels: regulation by calcium. *J. Bioenerg. Biomembr.* 23:537–560.
- McManus, O. B., L. M. H. Helms, L. Pallanck, B. Ganetzky, R. Swanson, and R. J. Leonard. 1995. Functional role of the β subunit of high conductance calcium-activated potassium channels. *Neuron.* 14:645–650.
- McManus, O. B., and K. L. Magleby. 1988. Kinetic states and modes of single large-conductance calcium-activated potassium channels in cultured rat skeletal muscle. *J. Physiol. (Lond.)* 402:79–120.
- McManus, O. B., and K. L. Magleby. 1991. Accounting for the Ca²⁺-dependent kinetics of single large-conductance Ca²⁺-activated K⁺ channels in rat skeletal muscle. *J. Physiol. (Lond.)* 443:739–777.
- Methfessel, C., and G. Boheim. 1982. The gating of single calcium-dependent potassium channels is described by an activation/blockade mechanism. *Biophys. Struct. Mech.* 9:35–60.
- Mienville, J.-M., J. L. Barker, and G. D. Lange. 1996. Mechanosensitive properties of BK channels from embryonic rat neuroepithelium. *J. Membr. Biol.* 153:211–216.
- Moss, B. L., S. D. Silberberg, C. M. Nimigeon, and K. L. Magleby. 1998. Mean open time can decrease and then increase with increasing intracellular calcium, suggesting a novel gating mechanism for a *dSlo* BK channel variant. *Biophys. J.* 74:217a. (Abstr.).
- Nelson, M. T., H. Cheng, M. Rubart, L. F. Santana, A. D. Bonev, H. J. Knot, and W. J. Lederer. 1995. Relaxation of arterial smooth muscle by calcium sparks. *Science.* 270:633–637.
- Petersen, O. H., and Y. Maruyama. 1984. Calcium-activated potassium channels and their role in secretion. *Nature.* 307:693–696.
- Reinhart, P. H., S. Chung, B. L. Martin, D. L. Brautigam, and I. B. Levitan. 1991. Modulation of calcium-activated potassium channels from rat brain by protein kinase A and phosphatase 2A. *J. Neurosci.* 11:1627–1635.
- Robitaille, R., M. L. Garcia, G. J. Kaczorowski, and M. P. Charlton. 1993. Functional colocalization of calcium and calcium-gated potassium channels in control of transmitter release. *Neuron.* 11:645–655.
- Rothberg, B. S., R. A. Bello, and K. L. Magleby. 1997. Two-dimensional components and hidden dependencies provide insight into ion channel gating mechanisms. *Biophys. J.* 72:2524–2544.
- Rothberg, B. S., R. A. Bello, L. Song, and K. L. Magleby. 1996. High Ca²⁺ concentrations induce a low activity mode and reveal Ca²⁺-independent long shut intervals in BK channels from rat muscle. *J. Physiol. (Lond.)* 493:673–689.
- Rothberg, B. S., and K. L. Magleby. 1998. Kinetic structure of large-conductance Ca²⁺-activated K⁺ channels suggests that the gating includes transitions through intermediate or secondary states: a mechanism for flickers. *J. Gen. Physiol.* 111:751–780.
- Schreiber, M., and L. Salkoff. 1997. A novel calcium-sensing domain in the BK channel. *Biophys. J.* 73:1355–1363.
- Sigworth, F. J., and S. M. Sine. 1987. Data transformations for improved display and fitting of single-channel dwell time histograms. *Biophys. J.* 52:1047–1054.
- Silberberg, S. D., A. Lagrutta, J. P. Adelman, and K. L. Magleby. 1996. Wanderlust kinetics and variable Ca²⁺-sensitivity of *dSlo*, a large conductance Ca²⁺-activated K⁺ channel, expressed in oocytes. *Biophys. J.* 70:2640–2651.
- Stefani, E., M. Ottolia, F. Noceti, R. Olcese, M. Wallner, R. Latorre, and L. Toro. 1997. Voltage-controlled gating in a large conductance Ca²⁺-sensitive K⁺ channel (hslo). *Proc. Natl. Acad. Sci. USA.* 94:5427–5431.
- Thuringer, D., and I. Findlay. 1997. Contrasting effects of intracellular redox couples on the regulation of maxi-K channels in isolated myocytes from rabbit pulmonary artery. *J. Physiol. (Lond.)* 500:583–592.
- Wu, Y. C., J. J. Art, M. B. Goodman, and R. Fettiplace. 1995. A kinetic description of the calcium-activated potassium channel and its application to electrical tuning of hair cells. *Prog. Biophys. Mol. Biol.* 63:131–158.